UNIVERSITY OF GENOA

Modeling Glioma Progression in Neural Organoids

PhD Thesis in

BIOTECHNOLOGY IN TRANSLATIONAL MEDICINE

Curriculum: Cellular and Molecular Biotechnology

XXXVIII Cycle

Supervisor:
Prof. Paolo Malatesta

Candidate:
Chiara Riviera

Academic Year

2024-2025

Index

Abstract

High-grade gliomas (HGG) are the most aggressive and heterogeneous brain tumors, with poor prognosis and limited therapeutic options. A major barrier to progress in HGG research is the lack of preclinical models that accurately capture tumor complexity and its interactions with the brain microenvironment. In this thesis, we explored neural organoid-based approaches to model gliomagenesis and tumor progression. We first optimized the generation of mouse neural organoids (mNO), which displayed organized neural rosettes, neurons, and astrocytes, recapitulating essential features of brain tissue. Using mNO, we tested two complementary strategies: (1) a cell-based approach, where primary murine glioma cells were introduced into organoids, and (2) a genetic-based approach, where PDGF-B was overexpressed using the PiggyBac transposon system to induce malignant transformation. While mNO provided a supportive microenvironment for mouse high-grade glioma cells (mHGG), sustaining their proliferation and stem-like properties, mouse low-grade glioma cells (mLGG) failed to engraft. Direct transplantation of tumor cells, tested on mHGG and confirming high engrafting, could be a promising strategy to model less invasive gliomas. In parallel, Platelet-Derived Growth Factor B (PDGF-B) overexpression generated proliferative tumor-like cells that express markers consistent with the ones expressed by gliomas in vivo. Finally, we started the transition to human neural organoids (hNO) to increase translational relevance. Transplanted mHGG cells successfully engrafted in hNO, forming heterogeneous tumor masses and interacting with microglia, which exhibited activation around tumor cells. Overall, this work demonstrates that neural organoids represent a versatile and physiologically relevant platform to study glioma biology, providing insights into tumor-microenvironment interactions and potential ways for therapeutic testing.

1 Introduction

1.1 Glioma

Glioma is the most frequent type of adult-type primary central nervous system (CNS) tumor[1]. Even though traditionally CNS tumor classification was based on histological features, more recently the classification took into consideration molecular biomarkers as well. Therefore, in the fifth edition of the World Health Organization (WHO) Classification of Tumors of the CNS (CNS5) the classification was revised to combine histopathological and molecular features for the most accurate classification. For instance, in CNS5 fourteen newly recognized types of tumors were added to the classification of gliomas, glioneuronal tumors and neuronal tumors thanks to the integration of data about the histopathological appearance and molecular features[2].

Gliomas, glioneuronal tumors and neuronal tumors were divided into six groups:

1) Adult-type diffuse gliomas, that represent most gliomas in adults and comprehend glioblastoma, IDH-wildtype.
2) Pediatric-type diffuse low-grade gliomas, in which are classified two of the newly recognized types of gliomas (diffuse astrocytoma, MYB or MYBL1-altered and Diffuse low-grade glioma, MAPK pathway-altered).
3) Pediatric-type diffuse high-grade gliomas, that are expected to behave more aggressively than pediatric-type low-grade gliomas. An example of glioma of this class is the diffuse midline glioma, H3 K27-altered.
4) Circumscribed astrocytic gliomas, that are opposed to diffuse glioma and display a more solid growth pattern.
5) Glioneuronal and neuronal tumors, that are characterized by neuronal differentiation.
6) Ependymomas, that are now classified on the basis of the anatomical site of the tumor as well.

1.1.1 High-Grade Gliomas (HGG)

Compared to the previous classification, CNS5 simplified the classification of adult-type diffuse gliomas. In particular, these gliomas were previously divided into 15 categories, mainly due to the fact that different grades were assigned to different entities. Currently, adult-type diffuse gliomas include three types of tumors, that can be differently graded based on histology and molecular features[2]:

- Astrocytoma, IDH-mutant, that can be graded as CNS WHO grade 2, 3 or 4.
- Oligodendroglioma, IDH-mutant and 1p/19q-codeleted, grade 2 and 3.
- Glioblastoma, IDH-wildtype, is the highest grade.

This classification has improved diagnostic accuracy and clinical relevance, particularly in distinguishing between tumors with distinct prognostic and therapeutic implications[3]. Within this framework, glioblastoma (GBM) represents the most aggressive and lethal form of adult-type diffuse gliomas. Glioblastoma (GBM) is the most common malignant primary brain tumor,

accounting for 14.2% of all tumors and 50.9% of malignant brain tumors. In USA, it has the incidence rate (3.27 per 100,000 population), with a predominance in males rather than in females (4.09 per 100,000 in males VS 2.55 per 100,000 in females). GBM is among the most commonly diagnosed tumors in older ages, together with meningiomas and pituitary tumors, with a median age at the diagnosis of 66 years. Among all malignant brain tumors, GBM is the one with the lowest median survival (8 months), with a five-year survival rate of 6.9%[4].

1.1.2 Standard-of-care for GBM treatment

The standard of care of GBM includes the surgical resection of contrast-enhancing tumor, followed by radiation plus concomitant and adjuvant temozolomide administration[5,6]. This regimen was adopted after a clinical trial involving 573 patients and 85 centers, in which it was demonstrated the increase of the median survival from 12.1 months with radiotherapy alone to 14.6 months with radiotherapy plus temozolomide[5]. Another study from the same group suggested the use of tumor-treating fields (TTFileds), that are low-intensity alternating electric fields delivered to the tumor that interferes with GBM cell division and organelle assembly. Indeed, the median survival of patients treated with maintenance TMZ and TTFields was 20.9 months, compared to 16.0 months for the group of patients treated with maintenance TMZ only[7]. Specific therapies are then considered depending on the characteristics of the tumor. For instance, it was observed that in patients with the methylation of MGMT (O6-methylguanine-DNA methyltransferase) promoter TMZ is more effective than in patients without the silencing of this promoter, with a median survival of 21.7 months for radiotherapy plus temozolomide compared to 15.3 months of radiotherapy alone[8].

Despite all the efforts, GBM recurrence is inevitable within 7 months[5], and a standard-of-care therapy has not been delineated yet. Surgery is rarely an option, due to the infiltration of the lesions. Systemic therapies may be applied, either rechallenges of TMZ and re-irradiation or new therapies such as treatment with bevacizumab and nitrosoureas. None of these therapies have proven effective in prolonging the survival of GBM patients[9].

1.1.3 Understanding GBM biology for novel treatments

To understand the reason why the standard of care therapies fails and to develop novel therapies, it is important to understand GBM biology.

1.1.3.1 Infiltration and integration of glioma cells in neural networks

Among the most well-known hallmarks of the disease, there is the diffuse infiltration of tumor cells, that is the main reason for impossibility to completely remove all the tumor cells with surgical resection and thus for GBM recurrence[10]. To understand the mechanisms underlying the migration and invasive capacity of GBM cells, we can look at the mechanisms of cell migration during neurodevelopment. For instance, migrating glioma cells express doublecortin (DCX), that is expressed by migrating neuroblasts and glial progenitors during development[11]. In the same way, myosin II is found to be expressed in the leading protrusion of glioma cells, supporting their motility[12] in a similar way that is used for soma translocation of neural progenitor cells during neurodevelopment[13]. Another molecular mechanism involved in GBM invasion is the formation of tumor microtubes (TMs), that increase in number with tumor

progression and are used by cell nuclei to travel after mitosis. The second role of TMs is to allow the formation of a multicellular network between malignant and non-malignant cells; this network is able to distribute among many different cell types the increase of intracellular calcium levels required for radiotherapy-induced cytotoxicity, leading to therapy resistance[12]. Possible therapeutic strategies to limit glioma invasiveness can be developed starting from this information about TMs. For instance, since gap junctions in TMs are involved in radiotherapy resistance, an inhibition of gap junctions-related proteins (such as GAP-43) can lead to increase radiosensitivity of the tumor. From another point of view, TMs can be exploited to distribute gap-junction permeable molecules even to distant, invasive tumor cells[14].

TM formation is dependent upon neuronal activity and neuronal inputs are given to glioma cells thanks to the formation of neuroglioma synapses[15,16]. In these synapses, glioma cells constitute the post-synaptic part, and they are excited via glutamate activation of AMPA receptors. The glutamatergic signals induce depolarization and intracellular calcium currents that induce tumor cell proliferation and invasion[16]. Indeed, epileptic seizures are a common comorbidity for patients with brain tumors, affecting as many as 75% of patients with glioma[6], and glutamate signal is involved in the imbalance of electrical activity[17]. So far only one anti-epileptic drug acting on AMPA receptors specifically (perampanel) is used in clinical practice, reducing seizure frequencies in patients with glioma[18]. However, data regarding its efficacy in reducing tumor growth are reported in preclinical models only[16,19].

The capacity of glioma cells to infiltrate brain tissue and integrate into functional neural circuits not only underlies tumor recurrence but also contributes to treatment resistance and neurological symptoms[1920,21]. A deeper understanding of the mechanisms that drive this pathological behavior can inform the development of targeted therapies.

1.1.3.2 Glioblastoma heterogeneity and cell states

While the infiltrative nature of GBM primarily accounts for the failure of surgical resection, its high molecular and cellular heterogeneity is the major cause for variable therapeutic responses and resistance to both radiotherapy and chemotherapy. The first attempt to dive into this heterogeneity was made when The Cancer Genome Atlas (TCGA) Research Network was established, with the aim of analyzing genomic alterations in a large cohort of 206 GBM samples to identify molecular prognostic and diagnostic markers[22]. Through this analysis, four molecular subtypes of GBM were identified, each of them associated with different molecular alterations and transcriptional profiles:

- Classical – characterized by chromosome 7 amplification paired with chromosome 10 loss, EGFR amplification and focal 9p21.3 homozygous deletion targeting CDKN2A. This subtype expresses genes associated with neural precursors signatures, such as NES, and pathways like Notch and Sonic hedgehog[22].
- Mesenchymal – characterized by low NF1 expression levels due to a focal hemizygous deletion of a region at 17q11.2. This subtype mainly expresses mesenchymal markers, such as MET, and genes related to the tumor necrosis factor super family pathway and NF-kB pathway. This is potentially reminiscent of an epithelial-to-mesenchymal

transition and to the consequent higher overall necrosis and associated inflammatory infiltrates usually found in this class[22].

- Proneural – characterized by PDGFRA amplification, point mutations in IDH1 and frequent TP53 mutations. The proneural subtype showed high expression of proneural development genes, such as SOX genes or DCX, but also high expression of oligodendrocyte development genes, such as PDGFRA and OLIG2[22].
- Neural – characterized by the expression of neuronal markers, such as NEFL and SYT1[22]. Due to its similarity to normal brain tissue, it was considered the result of normal brain cell contamination in the sequencing rather than a true tumor identity [20].

These subtypes exhibit differential responses to therapy. The mesenchymal subtype, in particular, is described as the most aggressive and the most related to resistance to primary radiotherapy[23] and to radiotherapy-induced resistance to TMZ[24]. The therapeutic resistance is the result of a phenomenon called proneural-to-mesenchymal transition (PMT), a process in which cells can undergo a dynamic transition between tumor subtypes in response to therapeutic stress. This plasticity was demonstrated in a proneural mouse model, where a mesenchymal shift occurred within 6 hours following radiation exposure[25]. Importantly, these subtypes can co-exist within the same tumor, as demonstrated by the fact that different regions of a single tumor can belong to distinct transcriptional subtypes[26], further complicating therapeutic targeting.

While these insights were initially obtained from bulk RNA sequencing, single cell RNA sequencing allowed the identification of a further layer of heterogeneity. In a study by Neftel and colleagues, four recurrent malignant cellular states were identified across GBM samples, each resembling a neural cell lineage: (1) mesenchymal-like (MES-like); (2) neural precursor cell-like (NPC-like); (3) astrocytic-like (AC-like); (4) oligodendrocytes precursor cell-like (OPC-like)[27]. Each cellular state has characteristics that largely correspond to the cell type they resemble, but with additional features that may reflect the distortion of these tumoral cellular states compared to normal cell type programs. The frequency of these 4 cellular states in tumors is influenced by copy number amplifications of the CDK4, EGFR and PDGFRA loci and by mutations in the NF1 loci. They also align with the transcriptional subtypes previously defined by Verhaak and colleagues: MES-like and AC-like states are enriched in mesenchymal and classical subtypes, respectively, while NPC-like and OPC-like states are combined in proneural tumors[27]. Since the intratumoral heterogeneity and plasticity of GBM present a major challenge to the development of effective treatments, understanding how different tumor cell populations evolve and interact within the tumor microenvironment is therefore essential[20,21].

1.2 Preclinical models of GBM

Despite significant advances in understanding the molecular and cellular biology of GBM, including its infiltrative nature, cellular plasticity and integration into neural circuits, the development of effective therapies remains elusive. One of the main barriers to translational progress is the limited capacity of traditional preclinical models to recapitulate the complex biological features of human GBM[28]. An ideal preclinical model of GBM should fulfill the following criteria to recapitulate the human disease: (1) have a genetic background that mirrors

human GBM or a GBM subtype; (2) maintain the genetic, epigenetic and phenotypic intratumoral heterogeneity, as well as tumor microenvironment, such as immune cells, blood-brain barrier (BBB) and physiologically relevant interactions between tumor and healthy cells in the brain; (3) be reproducible and stable over time[29].

Traditional preclinical models for GBM include in vitro/ex vivo and in vivo approaches, each of them with their own advantages and disadvantages that will be further discussed in the following chapters.

1.2.1 In vitro models of GBM

In vitro models of GBM primarily include tumor cell lines (of either mouse or human origin), tumoral spheroids and ex-vivo brain explants. These models are widely used in preclinical research due to their relatively low cost, ease of manipulation and suitability for high-throughput assays. However, the main limitations are the lack of the structure and microenvironmental complexity of in vivo models.

1.2.1.1 Tumor cell lines

Immortalized tumor cell lines are widely used in GBM research, and they are available from both murine and human sources. One of the first immortalized cell lines is the C6 cell line, developed by exposing astrocytes from outbred Wistar rats to N-methylnitrosourea for eight months[30]. Among murine models, the GL261 cell line, that was obtained from C56/BL/6 mice injected intracranially with 3-methylcholantrene[31], is frequently used, particularly in immunological studies, due to its weak immunogenicity[32]. As for the human cell lines, the most commonly used cell lines include U87[33] and U251, both derived from patient's tumor. While these lines have significantly contributed to our understanding of GBM biology[34], concerns have emerged regarding cross-contamination, genetic drift, and phenotypic alterations that accumulate over long-term culture[35]. Patient-derived primary GBM cell lines, while better reflect tumor heterogeneity, are more difficult to establish and, over time, even these cells will eventually drift in culture, losing some of the original tumor's characteristics[36].

In summary, tumor cell lines are valuable due to their affordability, ease of use, and long-term viability. Nonetheless, their lack of three-dimensional architecture, tumor microenvironment, and relevant cell-cell interactions limits their translational relevance.

1.2.1.2 Spheroids

To overcome the limitations of 2D cultures, tumor spheroids have been developed to better replicate the 3D structure of solid tumors. These models mimic better important physiological gradients, such as those of oxygen, nutrients, metabolites and drugs, providing insights not achievable in classical 2D monolayers[37].

Four main groups of spheroids can be identified:

1. Multicellular tumor spheroids, derived from single-cell suspension culture in conventional FBS-supplemented medium and non-adherent conditions. This model is mainly established using tumor cell lines[37].

2. Tumorospheres, composed of cancer stem cells cultured as free-floating spheres, usually in serum-free conditions and in a medium supplemented with growth factors. Tumorospheres were first described in the culture of brain tumors, and they were called neurospheres[38].
3. Tissue-derived tumor spheres, obtained from partially dissociated cancer tissue[37].
4. Organotypic multicellular spheroids, obtained from the culture of small ex vivo fragments without dissociation[37].

Spheroids overcome some limitations of 2D in-vitro models as they more accurately represent the 3D architecture and cell-cell interactions exhibited in solid tumors. But even in this case, they lack the complexity of the tumor microenvironment that is observed in vivo models[39].

1.2.1.3 Brain explants

Brain explants can be obtained either pre-mortem (during surgery), or post-mortem and provide another valuable ex vivo model. While pre-mortem brain explants are usually used for diagnostic purposes, they can also be cultured to preserve the native cytoarchitecture, offering a physiologically relevant platform for GBM research[40]. Conversely, post-mortem brain samples are useful to gain insights on end-stage disease, which is particularly of interest in understanding what drives the inevitable recurrence of GBM. However, their main limitation is the fact that usually the tissue is degraded due to the post-mortem interval[40].

Another particularly relevant ex vivo technique is the organotypic brain slice culture, which involves slicing mouse or rat brains and using them as a platform on which GBM cells can be incorporated. These slices preserve the native vasculature and immune components, that lack in the other most used in vitro models. However, the disadvantages are the short-term viability, and they are technically challenging in their preparation and maintenance[41].

1.2.2 In vivo models of GBM

Since the first use of rats as recipient for patient-derived transplanted tissue in the 1940s[42], animal models for primary brain cancers have provided researchers with the opportunity to investigate the cellular and molecular behavior of tumors in the context of a living organism. These models have been essential for advancing our understanding of tumor growth and biology, validating the efficacy and safety of drugs and treatments, and testing novel therapeutic approaches. Moreover, in vivo models retain physiologically relevant features that are important in neuro-oncology, such as the tumor microenvironment, angiogenesis, and immunological as well as inflammatory responses[43].

The main advantages of using murine models in neuro-oncology research are: (1) small and ease of handling; (2) rapid reproductive rate, facilitating long-term maintenance and experimentation; (3) fully characterized genome, enabling straightforward genetic manipulation[44]; (4) availability of numerous rodent-specific cell lines suitable for transplantation[43]. Despite these benefits, there is still the need for preclinical models that more accurately mimic human disease, as the translation of preclinical results into clinic is still suboptimal. The main reasons include anatomical differences between rodents and humans, such as the lack of gyrification and cortical development in the mouse brain[43]. These differences

must be taken into consideration both in the study of tumor biology and in the development of new therapeutic approaches and can be overcome by using other species for research. However, ethical concerns arise when working with species whose neuroanatomy more closely resembles that of humans, such as canine and non-human primates[45].

Animal models of GBM can be generated through two main approaches, that are the transplantation tumor cells or the genetic modification of the host animal[34,39,45]. As for the transplantation of tumor cells, when the transplanted cells are of murine origin, the model is referred to as syngeneic [45]; if the cells are of human origin, the model is called xenograft, that can be either cell line-derived or patient-derived[39]. While for the genetic modifications, this can be mediated by viral vectors, transposon systems, Cre-Lox or CRISPR-Cas9 genome editing approaches[34].

1.2.2.1 Syngeneic mouse models

Syngeneic mouse models are generated by transplanting tumor cell lines into genetically matched hosts. The most used cell lines are GL261 and CT2A, typically transplanted in C57BL/6 mice. The major advantage of this approach is the use of an immunocompetent host, which enables the study of tumor-immune system interactions and the evaluation of immunotherapies[46]. However, these models face two key limitations: (1) species limitations, that make direct translation of these findings to clinical applications difficult, and (2) the inability of immortalized lines to recapitulate the molecular and phenotypic heterogeneity of human GBM[46].

1.2.2.2 Xenograft mouse models

In contrast to syngeneic mouse models, xenografts mouse models involve the transplantation of human-derived tumor cells, requiring the use of an immunocompromised host to allow tumor growth[46]. Commonly used immortalized cell lines include U87 and U251, but these lines have undergone genotypic drift during long-term culture, resulting in a poor representation of GBM heterogeneity[46]. To address this, patient-derived xenograft (PDX) models became increasingly used. These models involve the transplantation of primary tumor cells derived from patients, that better retain the molecular, phenotypic and histopathological features of the original tumor, including its invasiveness, immunohistochemical profile, radiation sensitivity and response to TMZ[47]. Nevertheless, PDX also require immunocompromised mice, limiting their use for immunotherapy studies. One strategy to circumvent this is the development of humanized mouse models, in which the host immune system is replaced with a transplanted HLA-matched human immune system[46]. While promising, this approach is currently costly, labor-intensive and not suitable for long-term experiments, although future refinements may improve feasibility[46].

1.2.2.3 Viral vector-based transgenic mouse models

Viral vectors (including adenoviral (AdV), adeno-associated viral (AAV), lentiviral and retroviral vectors) are commonly used as a vehicle to introduce genes of interest into the host genome. Each vector type offers distinct advantages. AAV vectors exhibit low immunogenicity and are well-suited for in vivo applications, while AdV can infect both dividing and non-dividing cells and remain as episomes in the nucleus[34]. Lentiviral and retroviral vectors instead

integrate into the host genome, allowing stable expression, but carry a risk for insertional mutagenesis due to random integration[48].

Viral vectors can be administered through intravascular, intrathecal, intraventricular, and intracranial (via stereotaxic surgery) routes, without affecting the blood-brain barrier[34]. Administration can occur at embryonic or adult stages[34]. For example, our group developed a mouse model of glioma based on the overexpression of the Platelet-Derived Growth Factor B (PDGF-B) delivered using a retroviral vector in E14 embryos[49].

1.2.2.4 Transposon-based transgenic mouse models

To avoid viral-based methods, transposon systems provide a valid alternative. Transposons are mobile genetic sequences capable of inserting into various genetic locations[50]. They are considered safer than viral vectors, are cost-effective and present lower risk of insertional mutagenesis due to their lack of selective integration into genetic material[34]. Two main transposon systems are used for transgenic mouse models: Sleeping Beauty (SB) and PiggyBac (PB)[34].

The SB transposon is a synthetic transposon that operates via a cut-paste mechanism, in which the transposase enzyme excises and integrates the transgene flanked by direct/inverted repeats[51]. This system has been used to generate a mouse model of glioma that spontaneously developed intratumoral heterogeneity, by introducing a triple combination of platelet-derived growth factor subunit A (PDGFA) together with short-harpin RNA against *Nf1* and *Trp53*[52]. Another model was developed by using the SB transposon system into the lateral ventricle of neonatal mice ensuing ATRX knockdown collectively with H3.G34 mutation and IDH1-R132H mutation[53].

The PB transposon system uses two plasmids: one encoding the transposase and the other carrying the gene of interest flaked by inverted terminal repeats recognized by the enzyme[54]. Compared to SB system, PB transposons exhibit greater efficiency and have been used to generate GBM models with 100% tumor induction efficiency, for example via the electroporation of HRasV12 and AKT plasmid together with PBase expressed under the control of the GLAST promoter to facilitate the integration into glial precursor cells[55].

1.2.2.5 Cre-LoxP transgenic mouse models

The Cre-LoxP recombination system is based on the Cre recombinase enzyme, that catalyse which recognizes specific LoxP sequences and excises or activates genes located between them[56]. A typical approach involved crossing two mouse strains: one expressing the Cre recombinase and the other carrying the target gene or cassette flanked by two LoxP sites. By breeding these two animals together, the result is a model in which the Cre recombinase can cut out the sequence between the two sites, resulting in the deletion or activation (if the removed sequence was a stop sequence for a certain gene) of certain genes[45]. Cre-LoxP allows precise spatial control (via tissue-specific promoters)[45] and temporal control (via inducible systems such as tamoxifen- or tetracycline/doxycycline-dependent expression of Cre)[34].

For example, a GBM model with p53 deletion and PDGFRα overexpression was generated by crossing PDGFRα-overexpressing Cre mouse with a p53 floxed mouse[57]. Similarly, a cell-

specific tamoxifen-inducible Cre recombinase system was used to knock-out tumor suppressors known to be important in GBM, such as *Nf1*, *Trp53* and *Pten*, to investigate the cell of origin of the tumor[58].

1.2.2.6 CRISPR-Cas9 transgenic mouse models

The CRISPR-Cas9 gene editing technique is a widely used system to generate genetic modifications that is based a part of the bacterial adaptive immune system targeting the viral DNA from alien organisms[59]. Guided by a single-guide RNA (sgRNA), the Cas9 nuclease introduces a double-strand DNA break at a specific locus, which is then repaired either by non-homologous end joining (NHEJ)—creating knockouts—or homology-directed repair (HDR)—enabling knockins [60]. CRISPR-Cas9 offers a rapid and flexible way to activate or silence genes, making it especially suitable for modelling the multiple concurrent mutations characteristic of GBM[34]. However, off-target effects remain a limitation, highlighting the need for careful sg RNA design[61]. For example, retroviral delivery of CRISPR-Cas9 has been used to to generate mouse models of high-grade glioma that recapitulate the genetic heterogeneity of the disease, by deleting tumor suppressors such as Trp53, Cdkn2a and Pten and inducing mutations in BRAF V600E, frequently observed in various types of gliomas[62].

1.2.3 Bridging the gap: in vitro 3D organoid models

In the middle between traditional 2D in vitro systems and complex animal models, brain organoids represent an intermediate platform for studying disease. While animal models have long been used as valid systems for disease modelling and neuroanatomical studies, species-specific differences in brain architecture can limit their translational relevance. Conversely, standard in vitro cultures, although more species-specific, lack the structural complexity, cellular diversity and tumor microenvironment necessary to recapitulate brain tumor biology[63]. Organoids are 3D self-organizing structures capable of differentiating into different tissue-specific cell types[64]. Their key advantage lies in their ability to mimic, in vitro, both the architecture and certain functional aspects of their organ of origin[39]. This makes them particularly useful for bridging the gap between 2D cell cultures and in vivo animal models.

1.3 Neural organoids

Neural organoids are in vitro-generated cellular systems that emerge by self-organization of pluripotent stem cells (PSCs), capable of differentiating into multiple neural cell types and exhibiting cytoarchitectural and functional features reminiscent of brain or specific brain regions[64]. While PSCs cultured in adhesion have already demonstrated the capacity to self-organize forming rosette-like structures of primitive neuroepithelia[65], accurately modelling the complex architecture of the developing brain requires 3D growth. Early strategies employed a semi-3D culture system, such as the serum-free, floating culture of embryoid body-like aggregates (SFEB). In this approach, PSCs were aggregated into embryoid bodies (EBs), that were subsequently plated on coated dishes to differentiate into telencephalic progenitors. The addition of small molecules such as Wnt3a and Shh enabled direct differentiation into subregional dorsal and ventral telencephalic identities[66]. Initially developed with mouse embryonic stem cells (ESCs), the method was later adapted for human (ESC) by adding the

ROCK inhibitor Y-27632, which enhances PSCs survival[67,68]. Within the first week, polarized neuroepithelia formed on the EBs surface, eventually self-organizing into multiple small rosettes of neural precursors surrounding and growing around apical lumens[68]. Since then, numerous studies have developed organoids representing different regions of the nervous system. These can be can broadly classified according to the level of guidance, that is the addition of small molecules or factors during the differentiation, into two categories: (1) unguided organoids and (2) guided organoids[64].

1.3.1 Unguided neural organoids

Unguided differentiation, meaning without the addition of small molecules or factors, produces organoids with a high diversity of neural cell types, often representing different locations in the neural axis[64].

The most prominent example is the protocol described by Lancaster and Knoblich, in which this model was used to model human brain development and microcephaly[69]. The protocol involved four main steps:

1. EB generation: PSCs are dissociated into single cells and seeded into low-attachment 96-well plate, forming EBs or homogeneous size and morphology[69,70].
2. Neural induction: EBs are cultured in a minimal medium that selectively supports neuroectoderm development, preventing endodermal and mesodermal differentiation[69,70].
3. Static differentiation in Matrigel: EBs differentiated into neuroectoderm are embedded in Matrigel droplets, promoting the expansion of neuroepithelial buds.[69,70]
4. Dynamic differentiation: long-term culture in a spinning bioreactor or orbital shaker enhances nutrient and oxygen exchange, supporting further growth and development of brain regions[69,70].

In early stages, organoids should exhibit cells expressing Sox2 or Pax6 indicating the expanding neuroepithelium. After one month, neuronal differentiation becomes evident, with the expression of markers such as Tuj1 or DCX. After 2-3 months, different brain regions are visible, including forebrain marked by Foxg1, choroid plexus marked by TTR, hippocampus marked by Prox1 and Fzd9, ventral forebrain by Nkx2.1. Over time, neuronal populations increase, while progenitors decline. No information was provided on other cell types, since the glial populations were not characterized[69,70].

Later modifications to this protocol addressed some limitations. For instance, one of the issues was a strong “batch effect”, linked to variability between batches in terms of regional identity formation[71,72]. This was traced to differences in early neuroectoderm formation, and it was correlated with the abundance of non-neuronal mesoderm and endoderm cells[72]. To improve neuroectoderm organization and reproducibility, that in turn will ensure the formation of reliable neural identity, researchers increased the relative surface area of EBs, by either starting from EBs of smaller size or using fibrous micro scaffolds to generate shapes with higher surface area-to-volume ratios[72]. Another limitation common to 3D cultures is the formation of a necrotic core due to insufficient nutrients and oxygen diffusion. This was mitigated by

transitioning long-term culture of organoids to organotypic slice culture at the air-liquid interface, exposing the interior of the organoid to oxygen and media and therefore resulting in improvements in cell survival[73]. Moreover, this modification resulted in more morphological maturity, with neurons forming tracts similar to the ones of white matters after 1-2 months of culture[74]. Collectively, all these modifications were aimed at enhancing the reproducibility, the survival and the maturation of brain organoids.

Efforts were also focused on expanding the cellular diversity in the organoids. This is typically done by adding specific small molecules and factors to support the differentiation of stem and progenitor cells into the cell type of interest. For example, the addition of platelet-derived growth factor A (PDGF-A) and insulin growth factor 1 (IGF-1) promotes the proliferation and the survival of oligodendrocytes progenitor cells (OPC), while thyroid hormone (T3) induces oligodendrocytes differentiation and myelination[75,76]. Similarly, reducing the levels of the neuroectoderm stimulant heparin and delaying Matrigel embedding of the organoids preserves mesodermal progenitors, which can differentiate into microglia with phenotypic and functional similarity to their adult counterparts[77].

1.3.2 Guided neural organoids

Guided neural organoids model a specific region or domain of the nervous system by adding instructive signals that guide the generation of that specific region[64]. For example, hypothalamic organoids recapitulate part of the hypothalamus, retinal organoids mimic the retina, telencephalic organoids represent the telencephalon or forebrain, and cerebral cortical organoids resemble part of the dorsal forebrain[64].

A typical example of guided neural organoids is the generation of dorsal forebrain organoids, where neural induction is achieved through dual SMAD inhibition, using dorsomorphin and SB-431542 to inhibit the BMP and TGF-β signaling pathways. Progenitor proliferation is maintained by supplementing the culture with FGF2 and EGF, which are later replaced with brain-derived neurotrophic factor (BDNF) and neurotrophic factor 3 (NT3) to promote neuronal differentiation[78]. Ventral forebrain organoids also employ dual SMAD inhibition, but with the addition of IWP-2 (a Wnt pathway inhibitor), and SAG (a SHH pathway agonist), while long-term differentiation similarly relies on BDNF and NT3[79].

Other examples of region-specific guided neural organoids include:

- Hippocampal organoids: generated via treatment with a GSK3 inhibitor and BMP4. After long-term culture these organoids gave rise to functional hippocampal neurons[80].
- Thalamic organoids: induced via dual SMAD inhibition was to drive the neuroectodermal fate and insulin treatment for caudalization, reflecting the caudal forebrain origin of the thalamus. This was followed by PD0325901 treatment (a MEK-ERK inhibitor) to prevent an excess caudalization toward midbrain cell fate and BMP7 to promote thalamic differentiation[81].
- Hypothalamic organoids: produced by SMAD inhibition to generate neural precursors, followed by the addition of WNT3A, SHH, and Purmorphamine to induce the hypothalamic differentiation[82].

- Midbrain organoids: patterned toward a mesencephalic fate by applying SHH agonists, FGF-8, SMAD inhibitors and GSK3b inhibitor (Wnt pathway activator)[82,83].
- Cerebellar organoids: derived through TGF-β inhibition and supplementation with FGF2 and insulin to produce cerebellar progenitors. Later during the differentiation, the subsequent addition of FGF19 and SDF1 promoted the formation of a thick neuroepithelial structure with flat-oval shape and enhanced the continuity of the cortical plate neuroepithelium[84].
- Striatal organoids: obtained by modulating SMAD and WNT pathways, and by adding activin A and an agonist of retinoid X receptor gamma (RXRG, highly expressed in the early developing human striatum) that promote the striatal differentiation[85].
- Hindbrain/cervical spinal cord organoids: produced via dual SMAD inhibition to induce neuroectoderm formation, followed by treatment with retinoic acid, and FGF-2 (modulators expressed along the rostro-caudal axis) and SAG (agonist of SHH, that is expressed along the dorso-ventral axis)[86].

A major advantage of guided organoids is the possibility to model inter-regional interactions by combining distinct domains. For example, dorsal and ventral forebrain organoids can be fused to study the saltatory migration of interneurons toward the cerebral cortex[79]. The integration of multiple organoids results in a new 3D cellular system, called assembloid, that further increases the levels of complexity of the in vitro modeling[64]. Moreover, guided neural organoids tend to be more reproducible and less heterogeneous than unguided neural organoids, reducing the batch-effect[87].

1.3.3 Translating neural organoids into disease modelling

Brain organoids can reproduce several key features of the human brain, including cellular composition and organization, physiological architecture, electrical activities and neuronal networks[69,82]. Their ability to recapitulate the development of the fetal brain[88] makes them particularly suitable for modelling neurodevelopmental disorders, in which processes such as premature differentiation, reduced proliferation and cell cycle disruption, are often altered and accurately represented in brain organoids[89]. Although neurodegenerative diseases can also be studied with organoids, the lack of aging remains a major limitation, especially for late-onset and age-related conditions[87]. More recently, organoids raised have emerged as promising tools for the study of neuropsychiatric disorders, providing new opportunities to explore disease biology and to identify dysregulated pathways[90].

1.3.3.1 Modelling of neurodevelopmental disorders

The use of organoids for the modelling of neurodevelopmental disorders is particularly useful since their generation recapitulates the stages of brain development. For example, the unguided neural organoid differentiation protocol was applied to study primary microcephaly[69]. In this specific case, organoids were obtained from induced pluripotent stem cells (iPSCs) derived from microcephaly patients carrying mutations in mitosis-associated genes that resulted in the dysregulation of the cell division plane and early depletion of neural progenitor cells, ultimately resulting in smaller organoids[69]. Similarly, organoids derived from a Seckel syndrome patient, another microcephaly-associated condition caused by mutations in the centrosomal-P4.1-

associated protein (CPAP), displayed reduced dimensions and a premature neuronal differentiation[91]. Not all cases of microcephaly are genetic; environmental factors such as infections can also trigger the condition. Organoids are valuable in such context because they can be experimentally exposed to the environmental factor, allowing direct observation of the phenotypic consequences[89]. For instance, forebrain organoids infected with Zika virus (ZIKV) at day 14 of differentiation to model the infection of the virus during pregnancy showed a reduction in ventricular zone thickness and size, combined with a significant increase of the lumen of the ventricular structures. This phenotype closely resembles the ventricular dilatation observed in affected foetuses[82]. In early 2016, a causality between SIKV infection and congenital microcephaly was not demonstrated yet, despite a correlation between the SIKV epidemic and an increase in cases of congenital microcephaly; studies on organoids helped in the identification of the link[92,93]. However, these investigations also revealed some limitations of organoid models: while both organoids and primary human tissue demonstrated infection of neural progenitors, discrepancies emerged regarding astrocytes susceptibility (observed in primary tissue but only occasionally in organoids) and microglial vulnerability (not detected in organoids)[94], likely because both cell types are under-represented or completely absent in some types of neural organoids.

In other disorders, when major phenotypic alterations are absent, the modelling can be more difficult but organoids still offer advantages compared to the animal model. For example, Miller-Dieker syndrome (MDS), a severe form of lissencephaly[89], cannot be effectively studied in mice due to their naturally smooth cortex[95]. Although current organoids do not fully recapitulate the human cortical folding, they contain cell types and developmental programs necessary to investigate the disease, such as an outer proliferative zone containing abundant outer radial glia cells (oRG) that are lacking in rodents[96,97]. This for instance allowed for the identification in organoids derived from lissencephaly patients of an impaired division of oRG that remain in mitosis for much longer period of time compared to controls[98]. Advances in organoid complexity will allow for more precise investigation of developmental disorders involving abnormal cortical folding. For instance, deletion of the PTEN gene, linked to human macrocephaly, in both mouse and human neural organoids resulted in increased size, but only human organoids displayed neuroepithelial overgrowth and enhanced surface convolution, a phenotype rescued by viral delivery of wild-type PTEN[99]. Such findings underline the human-specific developmental processes that organoids can reveal, providing unique insights inaccessible through conventional animal models.

1.3.3.2 Modelling of neuropsychiatric disorders

Neural organoids have been widely employed to model neuropsychiatric disorders, mainly to investigate how specific genetic variants influence disease susceptibility and alter key biological pathways[90].

One of the most studied conditions is autism spectrum disorder (ASD), a heterogeneous neuropsychiatric disorder characterized by varying degrees of impairment in communication and social interaction, repetitive or restrictive behaviors, language difficulties, lack of social and emotional relationships, apathy, and others[100]. This clinical heterogeneity is mirrored at the genetic level, representing a major challenge for developing models capable of capturing the

full spectrum of genetic heterogeneity[101]. The prevalent approach involved generating patient-derived organoids from ASD to compare molecular and developmental alterations with healthy controls. This strategy has provided key insights into how specific mutations affect neural development. For example, overexpression of the transcription factor FOXG1, a modification observed in some idiopathic ASD forms, leads to increased production of inhibitory neurons[102]. Similarly, the deletion of duplication of the 16p11.2, the most common copy number variation in ASD, have been shown to alter synapse number, neuronal proliferation and maturation and overall organoid size[103].

Since the disrupted functional connectivity is a hallmark of ASD, neural organoids models were developed to replicate and study these network-level deficits. For instance, iPSCs from patients with Timothy syndrome, a severe neuropsychiatric disease characterized by ASD and epilepsy, were differentiated into dorsal and ventral forebrain organoids, that were subsequently fused together to mimic interneuron migration. This model revealed a cell-autonomous migration defect in Timothy syndrome-derived interneurons[79].

1.3.3.3 Modelling of neurodegenerative disorders

Although neural organoids typically resemble the developing brain, they can still serve as valuable platforms for studying neurodegenerative diseases, particularly when they reproduce relevant pathological hallmarks. These models can elucidate disease mechanisms and help to create new therapeutics[104].

For example, Alzheimer's disease (AD) is characterized by the deposition of extracellular plaques of amyloid-beta (Aβ) peptides and intracellular neurofibrillary tangles made of hyperphosphorylated aggregates of the microtubule-associated protein tau[105]. Neural organoids have been used to first demonstrate the link between the excessive accumulation of Aβ and the formation of neurofibrillary tangles, something that was not achievable in traditional models. Indeed, mouse models of familial AD could reproduce Aβ plaques but not neurofibrillary tangles deposition, and neurons derived from AD patients lacked both[106,107].

After AD, the second most common neurodegenerative disease is Parkinson's disease (PD), that is characterized by the progressive loss of dopaminergic neurons in the substantia nigra, leading to motor symptoms such as resting tremor and bradykinesia[108]. The main pathological characteristic of PD is α-synuclein inclusions (Lewy bodies)[109], and the most common mutation associated to late-onset familial and sporadic PD is a missense mutation on the leucine-rich repeat kinase 2 (LRRK2) gene locus[110]. As with AD, animal models show limitations; for example, LRKK2-mutant animals fail to exhibit dopaminergic neuron loss or Lewy body formation[111]. By contrast, midbrain organoids derived from iPSC containing a mutation in LRRK2 successfully recapitulated key pathological signatures observed in PD patients carrying this mutation, including increased aggregation of α-synuclein and impaired clearance[112].

1.4 Neural organoids in neuro-oncology

Brain organoids represent a promising platform in neuro-oncology because they can bridge the gap between traditional in vitro and in vivo models. The lack of models capable of faithfully

reproducing the complexity of brain tumors is one of the key aspects holding back the investigation of tumor biology and the development of novel treatments[28]. Neural organoids are advantageous because they can maintain multiple cellular lineages and preserve complex cell-cell communication[113]. Importantly, they retain the genetic and phenotypic heterogeneity of the parental tumors[114,115], while also enabling the study of tumor behavior within a human-specific microenvironment[116]. Two main neural organoid-based models are currently employed in neuro-oncology: (1) transplantation models, in which tumor cells are introduced into PSCs-derived neural organoids by co-culture or transplantation; (2) in which genetic alterations are directly introduced into healthy organoid cells to drive neoplastic transformation[39,116].

1.4.1 Transplantation model

Transplantation models are based on the co-culture of tumor cells with neural organoids, thus containing both malignant and non-malignant cells. This model enables the maintenance of the tumor microenvironment (TME) interactions and allows the investigation of tumor invasiveness and TME-driven tumor promoting mechanisms. These models also serve as a valuable platform for evaluating the effectiveness of therapeutic interventions targeting invasion, a hallmark of GBM[117–119].

Two main approaches have been developed:

1. Co-culture of glioma stem cells (GSCs) with pre-formed neural organoids, resulting in integration and proliferation of tumor cells and the formation of tumor-like structures resembling patients' GBM[117,118].
2. Fusion of tumor spheroids with neural organoids, producing assembloids in which tumor cells infiltrate organoid tissue[119].

The most famous transplantation model for GBM research was the cerebral organoid glioma (GLICO) model developed by Linkous and colleagues[117]. In this system, glioma stem cells (GSCs) were co-cultured with neural organoids, generating tumors that preserve histopathological and molecular features that are similar to surgical and autopsy specimens, maintaining patient-specific EGFR amplification and phosphor-RTK signaling, as well as the spontaneous formation of microtubes. These microtubes create a network enabling communication among tumor cells and between tumor and healthy neural cells, driving invasion and progression[116,117,120]. The ability to study such phenomena in a manipulable in vitro system is highly valuable for both mechanistic studies and therapeutic targeting.

GLICO has also proven useful for drug screening, since TME influences treatment response. Using GLICO, Linkous and colleagues were able to demonstrate that GSCs cultured within organoids displayed greater resistance to drug and radiation-induced genotoxic stress compared to 2D culture conditions, underlying the importance of taking into account TME when running drug screenings[117]. Furthermore, the coexistence of malignant and non-malignant cells allows simultaneous assessment of therapeutic efficacy and neurotoxicity. For example, the drug UM-002 tested in GLICO showed GBM-specific cytotoxicity at low doses while sparing neural organoid tissue, but induced toxicity in both populations at higher

concentrations[121]. Such observations highlight the translational potential of organoid models in preclinical drug development and toxicity evaluation.

Nevertheless, transplantation models have limitations. Tumor establishment time varies depending on neural organoid maturation stage, and immune as well as vascular components of the TME are largely absent[116].

1.4.2 Transduction model

Transduction models are based on the induction of oncogenic alterations within healthy neural organoid cells, typically through oncogene overexpression or tumor suppressor gene inactivation. These models are useful for studying the role of genetic drivers in tumor initiation and progression[116], and for generating tumors with genetic profiles similar to GBM patients[39]. Genetic modifications are most often introduced using transposon-based systems for gene activation and CRISPR-Cas9 for gene knockout[122–124].

A proof-of-concept study demonstrated that introducing $HRas^{G12V}$, alongside TP53 loss into neural organoids triggered the emergence of highly proliferative, invasive tumor cells. These cells rapidly replaced normal organoid tissue and were tumorigenic when transplanted into mice, ultimately leading to animal death[124]. Interestingly, cell lines that failed to kill mice also failed to invade the organoid tissue, indicating the predictive power of neural organoids for tumor invasiveness and lethality[124]. While this specific mutational combination was not fully representative of GBM genetics, the study established the feasibility of this approach[124].

In parallel, another study published in the same year showed the recapitulation of genetic modifications found in people with brain cancers in neural organoids, generating new in vitro model system for human brain tumors that were called neoCORs[123]. Using a four-plasmid electroporation system, researchers combined: (1) Sleeping Beauty (SB) transposase for genomic integration; (2) GFP for cell tracing; (3) an oncogene construct for overexpression; (4) plasmids encoding for Cas9 nuclease together with sgRNAs for tumor suppressor knockout. This allowed to have a flexible system to introduce any combination of gain or loss of function mutations[123]. Within one month, organoids carrying GBM-relevant mutations, such as $CDKN2A^{-/-}/CDKN2B^{-/-}/EGFR^{OE}/EGFRvIII^{OE}$, $NF1^{-/-}/PTEN^{-/-}/TP53^{-/-}$ ($p53^{-/-}$) and $EGFRvIII^{OE}/CDKN2A^{-/-}/PTEN^{-/-}$, developed proliferative tumor masses. Notably, MYC overexpression (MYC^{OE}) generated tumors resembling primitive neuroectodermal tumors (CNS-PNET), for which no in vitro or animal model previously existed[123].

Compared with GLICO, neoCORs also include both tumor and non-tumor cells, permitting interaction studies and therapeutic testing. However, their unique advantage lies in modeling tumor initiation, even though more complexity should be reached given the heterogeneity typical of GBM[123]. Genetic modifications have also been introduced into guided neural organoids, as shown by Lago and colleagues, who generated high-grade glioma and medulloblastoma organoids by electroporating forebrain and cerebellum organoids respectively[122].

Despite their potential, transduction models face challenges: long establishment times, lack of immune and vascular cells, difficulties in fully capturing tumor heterogeneity, and possible off-target or unanticipated effects of the artificially introduced genes on gene expression[116].

2 Rationale

In our group, glioma progression was studied in an animal model based on the transduction of the Platelet-Derived Growth Factor B (PDGF-B) in E14 mice brains[49]. The developing tumors undergo progression from low grades (mLGG) to high grades (mHGG). mLGG and mHGG are distinguished based on histopathological features and on the tumorigenic potential when injected into syngeneic mice. mHGG explanted 100 days after birth are tumorigenic, while mLGG, explanted within 60 days from birth, do not give rise to secondary tumors when transplanted in syngeneic mice[49] [Figure 1a]. Previous studies showed that this lack of tumorigenic potential is mainly due to their immunostimulatory properties. In fact, when mLGG were transplanted in NOD/SCID mice, they succeeded in generating a secondary tumor. However, when these tumors are transplanted in immunocompetent mice, they generated tertiary tumors[125] [Figure 1b]. This suggests that immune selective pressure alone is unlikely to fully account for tumor progression. These data indicated that in PDGF-B-induced gliomas malignancy is acquired over time, with a latency of about 90 days. Further experiments focused on clonal dynamics revealed a significant reduction in the number of clones during the progression from low grade to high grade[126]. This implies that mHGG are constituted of a limited number of clones that underwent the clonal selection during the tumor progression. Consequently, when mHGG are transplanted into syngeneic mice, they should not undergo further clonal selection. However, transplantation experiments demonstrated that the clonal selection happens even in this case[126]. It is still unclear whether post-transplantation selection mirrors the one occurring during the progression from low to high grades.

Despite the insights gained from this animal model, some critical aspects remain unresolved. Studying mLGG is particularly challenging, as these cells cannot be maintained in culture, requiring de novo induction in embryos each time. This approach is costly, labor-intensive, and ethically problematic. Similarly, dissecting the very early events of gliomagenesis is difficult because tumors are initially too small to be detected, and continuous monitoring in vivo is not feasible. To address these limitations, we established an in vitro glioma model based on neural organoids. The first part of this work was focused on developing a model based on mouse neural organoids (mNO), to establish and optimize the methodology in a system aligned with our animal model, allowing us to refine approaches and address specific questions that emerged from the in vivo work. Once the platform was established, our aim was to transition to human neural organoids (hNO), for investigating the glioma progression in a more translational model [Figure 1c].

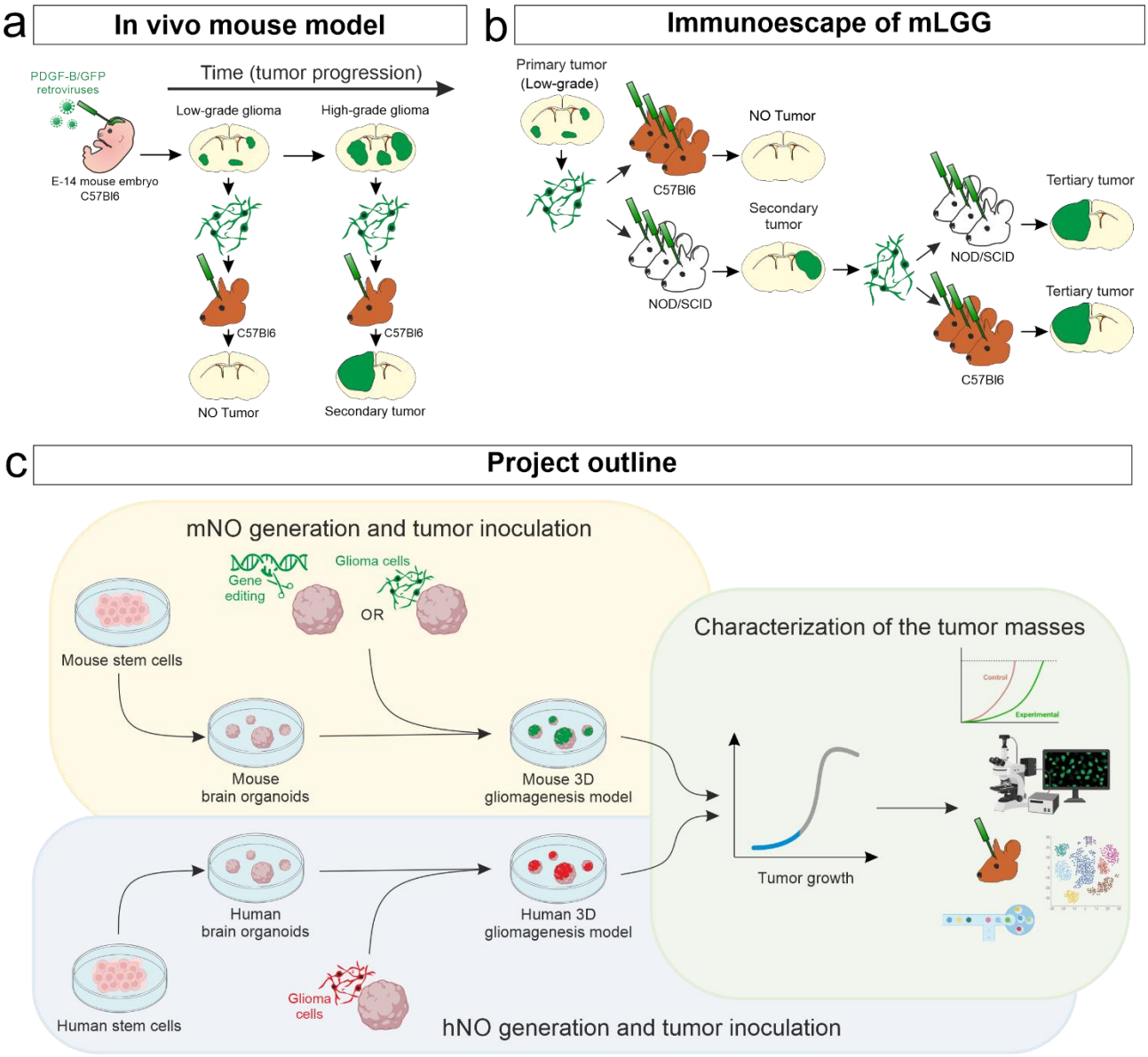

Figure 1. Rationale and project outline. (**a**) In vivo mouse glioma model. The mouse model used in our laboratory is based on the overexpression of PDGF-B in mouse embryos at E14. Following injections, mice develop gliomas that progress over time from low-grade glioma (mLGG) to high-grade glioma (mHGG). These tumor stages differ in their histopathological features and in their tumorigenic capacity when transplanted into syngeneic mice: while mHGG readily generate secondary tumors, mLGG fail to do so. (**b**) Immunoescape of mLGG. Despite their inability to engraft in immunocompetent host, mLGG can form secondary tumors when transplanted into immunodeficient NOD/SCID mice. Cells derived from these secondary tumors underwent progression and acquire tumorigenic potential, since they are able to generate tertiary tumors when transplanted into immunocompetent mice. (**c**) Project outline. To overcome the limitations of the in vivo model, the aim of the project was to develop a complementary in vitro platform based on neural organoids. First, mouse neural organoids (mNO) have been generated and used to establish glioma models either by genetic engineering or by inoculation of glioma cells. Tumor growth was monitored and characterized over time. Once validated, the system was extended to human neural organoids (hNO), to provide a translationally relevant model of gliomagenesis.

3 Materials and Methods

3.1 Cell culture

Primary cultures of glioma cells, derived from dissociation of murine gliomas, were cultured in Matrigel (BD Biosciences) coated flasks using DMEM/F12 medium (Thermo Fisher Scientific) supplemented with 1:50 B27 (Thermo Fisher Scientific), 10 ng/ml recombinant human FGF2 (PreproTech), 10 ng/ml recombinant human EGF (PreproTech) and Penicillin-Streptomicin (Thermo Fisher Scientific).

Neural progenitor cells (NPC), derived from embryos at embryonic day 14, were cultured in Matrigel (BD Biosciences) coated flasks using DMEM/F12 medium (Thermo Fisher Scientific) supplemented with 1:50 B27 (Thermo Fisher Scientific), 10 ng/ml recombinant human EGF (PreproTech) and Penicillin-Streptomicin (Thermo Fisher Scientific). For the experiments described in the paragraph 4.1.3 "Mouse neural organoid derivation from neural precursor cells", NPC were cultured in GMEM medium (Thermo Fisher Scientific) supplemented with 10% FBS (Thermo Fisher Scientific), 1000 U/ml LIF (MedChem Express), 1mM sodium pyruvate (Euroclone), 0.05 mM beta-mercaptoethanol (Thermo Fisher Scientific), 1mM MEM non-essential amino acids (Thermo Fisher Scientific).

Mouse embryonic stem cells (mESC) E14Tg2A were cultured in Matrigel coated flasks. Cells were thawed in GMEM medium (Thermo Fisher Scientific) supplemented with 10% FBS (Thermo Fisher Scientific), 1000 U/ml LIF (MedChem Express), 1mM sodium pyruvate (Euroclone), 0.05 mM beta-mercaptoethanol (Thermo Fisher Scientific), 1mM MEM non-essential amino acids (Thermo Fisher Scientific) and subsequently cultured in GMEM medium supplemented with 1:50 B27 without vitamin A (Thermo Fisher Scientific), 1:100 N2 (Thermo Fisher Scientific), 1000 U/ml LIF (MedChem Express), 1μM PD0325901 (MedChem Express), 3 μM CHIR99021 (MedChem Express), 1mM sodium pyruvate (Euroclone), 0.05 mM beta-mercaptoethanol (Thermo Fisher Scientific), 0.1 mM MEM non-essential amino acids (Thermo Fisher Scientific).

Human induced pluripotent stem cells (hiPSC) ISFi001-A were cultured in Geltrex (Thermo Fisher Scientific) coated 6-well plates in mTeSR medium (Stem Cell Technologies), with daily media changes.

3.2 Neural organoid generation

3.2.1 Mouse neural organoids

On day 0, mESC were dissociated into single cells using trypsin 0.05% (Thermo Fisher Scientific) and 3000 of them were seeded in U-shape Ultra Low Attachment (ULA) 96-well plate (Corning) in 150μl of one of these media: 1) GMEM medium (Thermo Fisher Scientific) supplemented with 10% FBS (Thermo Fisher Scientific), 10 μM SB431542, 1mM sodium pyruvate (Euroclone), 0.05 mM beta-mercaptoethanol (Thermo Fisher Scientific), 0.1 mM MEM non-essential amino acids (Thermo Fisher Scientific); 2) GMEM medium (Thermo Fisher

Scientific) supplemented with 1:50 B27 without vitamin A (Thermo Fisher Scientific), 1:100 N2 (Thermo Fisher Scientific), 1000 U/ml LIF (MedChem Express), 1 μM PD0325901 (MedChem Express), 3 μM CHIR99021 (MedChem Express), 1 mM sodium pyruvate (Euroclone), 0.05 mM beta-mercaptoethanol (Thermo Fisher Scientific), 0.1 mM MEM non-essential amino acids (Thermo Fisher Scientific). Media change was performed on day 4. On day 6, EB media was changed with the neural induction media, composed of DMEM/F12 media (Thermo Fisher Scientific) supplemented with 1:100 N2 (Thermo Fisher Scientific), 1μg/ml heparin (Sigma), 0.1 mM MEM non-essential amino acids (Thermo Fisher Scientific). Media was changed on day 8 and on day 11 it was switched to differentiation media without vitamin A, composed of 1:1 DMEM/F12 and Neurobasal media (Thermo Fisher Scientific), supplemented with 1:100 B27 without vitamin A (Thermo Fisher Scientific), 1:200 N2 (Thermo Fisher Scientific), 2.5 ng/ml insulin (Sigma), 0.05 mM beta-mercaptoethanol (Thermo Fisher Scientific), 0.1 mM MEM non-essential amino acids (Thermo Fisher Scientific). Media was changed on day 13. On day 15, NO were moved from 96-well plate to petri dishes and kept in agitation (50 rpm) in differentiation media with vitamin A, composed of 1:1 DMEM/F12 and Neurobasal media (Thermo Fisher Scientific), supplemented with 1:100 B27 (Thermo Fisher Scientific), 1:200 N2 (Thermo Fisher Scientific), 2.5 ng/ml insulin (Sigma), 0.05 mM beta-mercaptoethanol (Thermo Fisher Scientific), 0.1 mM MEM non-essential amino acids (Thermo Fisher Scientific). From day 15 on, media was changed twice a week and mNO were maintained under agitation until day 30, when they were used for further processing.

3.2.2 Neural organoids from NPC

On day 0, NPC were dissociated to single cells using trypsin (Thermo Fisher Scientific) and seeded at a concentration of 9000 cells per well in a ULA 96-well plate to form EBs. Two different media composition were tested: 1) DMEM/F12 medium (Thermo Fisher Scientific) supplemented with 1:50 B27 (Thermo Fisher Scientific), 10 ng/ml recombinant human FGF2 (PreproTech), 10 ng/ml recombinant human EGF (PreproTech) and Penicillin-Streptomicin (Thermo Fisher Scientific); 2) GMEM medium (Thermo Fisher Scientific) supplemented with 10% FBS (Thermo Fisher Scientific), 1000 U/ml LIF (MedChem Express), 1mM sodium pyruvate (Euroclone), 0.05 mM beta-mercaptoethanol (Thermo Fisher Scientific), 1mM MEM non-essential amino acids (Thermo Fisher Scientific). After 4 days, EBs were directly embedded in Matrigel and cultured in differentiation media without vitamin A, composed of 1:1 DMEM/F12 and Neurobasal media (Thermo Fisher Scientific), supplemented with 1:100 B27 without vitamin A (Thermo Fisher Scientific), 1:200 N2 (Thermo Fisher Scientific), 2.5 ng/ml insulin (Sigma), 0.05 mM beta-mercaptoethanol (Thermo Fisher Scientific), 0.1 mM MEM non-essential amino acids (Thermo Fisher Scientific).

3.2.3 Human neural organoid

To obtain human neural organoids (hNO), iPSC were dissociated to single cells using accutase (Sigma-Aldrich) and seeded at a concentration of 9000 cells per well in a ULA 96-well plate to form embryoid bodies. iPSC were seeded in DMEM/F12 (Thermo Fisher Scientific) supplemented with 20% Knock-Out replacement serum (Thermo Fisher Scientific), 3% ES-quality FBS (Thermo Fisher Scientific), 0.1 mM MEM non-essential amino acids (Thermo Fisher

Scientific), 0.025 mM beta-mercaptoethanol (Thermo Fisher Scientific), 1:200 rock inhibitor Y27632 (VWR) and 4 ng/ml recombinant human FGF2 (PreproTech). On day 3, media was changed with low FGF medium without rock inhibitor Y27632 and recombinant human FGF2. On day 5, embryoid bodies were directed toward either dorsal or ventral neural induction by changing the media in neural induction media (NIM) with or without patterning molecules. For dorsa identity, NIM without the addition of small molecules was used: DMEM/F12 (Thermo Fisher Scientific), 1:100 N2 (Thermo Fisher Scientific), 1 mM MEM non-essential amino acids (Thermo Fisher Scientific) and 0.1 μg/ml heparin (Sigma-Aldrich). For ventral identity, NIM was supplemented with 0.1 μM SAG and 2.5 μM IWP-2. Media was changed every other day until day 13, on which patterned embryoid bodies were fused together via Matrigel (BD Biosciences) embedding. One dorsal and one ventral organoid were placed in a Matrigel droplet and moved to be close one to the other. Once the Matrigel droplet solidified at room temperature, the embedded organoids were transferred in petri dishes with improved differentiation media without vitamin A, composed of 1:1 mixture of DMEM/F12 and Neurobasal (Thermo Fisher Scientific), 1:200 N2 supplement (Thermo Fisher Scientific), 1:100 B27 without vitamin A, 2.5 μg/ml insulin (Sigma-Aldrich), 0.025 mM beta-mercaptoethanol (Thermo Fisher Scientific), 0.5 mM MEM non-essential amino acids (Thermo Fisher Scientific) and Penicillin-Streptomicin (Thermo Fisher Scientific). On day 17, the fused organoids were transferred to an orbital shaker in improved differentiation media with vitamin A and maintained under agitation (50 rpm) until day 105-110, when they were transplanted with tumor cells.

3.3 Co-culture of glioma cells with NO

For the establishment of co-culture, three different methods were evaluated. In all of them, mHGG were initially dissociated into single cells with trypsin.

1. In the first method, each NO was in an individual well of a 24-well plate. Subsequently, 10.000 mHGG were added per well in DMEM/F12 medium (Thermo Fisher Scientific) supplemented with 1:50 B27 (Thermo Fisher Scientific), 10 ng/ml recombinant human FGF2 (PreproTech), 10 ng/ml recombinant human EGF (PreproTech) and Penicillin-Streptomicin (Thermo Fisher Scientific). After 24 hours, NO were washed with 1X PBS and transferred to a new 24-well plate, where they were maintained under agitation for long-term culture.
2. In the second method, NO were seeded individually in a ULA 96-well plate and co-cultured with 5000 tumor cells per well in the same supplemented DMEM/F12 medium. After 24 hours, the organoids were washed with 1X PBS and transferred to petri dishes under continuous agitation for long-term maintenance.
3. In the third method, 3000 mHGG cells were seeded into ULA 96-well plate one day priori to co-culture to allow the formation of tumor spheroids. On the following day, NO were added to each well. After 48 hours, the resulting fused assembloid were transferred to petri dishes and maintained under agitation for extended culture.

The second method was selected for all the subsequent experiments.

3.4 Transplantation of mHGG in NO

mHGG were dissociated into single cells using trypsin 0.05% (Thermo Fisher Scientific) and resuspended in DMEM/F12 medium (Thermo Fisher Scientific) supplemented with 1:50 B27 (Thermo Fisher Scientific), 10 ng/ml recombinant human FGF2 (PreproTech), 10 ng/ml recombinant human EGF (PreproTech) and Penicillin-Streptomicin (Thermo Fisher Scientific). For the microinjection, NO were placed in droplets of differentiation media with vitamin A in a petri dish to limit their movement during the injection process. Tumor cells were adjusted to a concentration of 2000 cells/μl and 1 μl was injected into each organoid using a Nanoject microinjector under a stereomicroscope, within a biosafety cabinet. Following injection, fresh medium was, and organoid were maintained overnight without agitation. On the following day, the medium was replaced to remove non-integrated tumor cells, and the petri dishes were transferred to agitation conditions for long-term culture.

3.5 Electroporation of NO

Organoids were electroporated using the Neon NxT electroporation system (Thermo Fisher Scientific) and the Neon 100 μl transfection kit, according to manufacturer's instructions. The electroporation parameters were set as follows: pulse volt 1150 V, pulse width 30 ms and pulse number 2. Each electroporation was performed with a total of 5 μg DNA, consisting of a 1:1 mixture of pRP-CAG-hyPBase (Vector Builder), which encodes the transposase enzyme, and pPB-CAG-hPDGFB-IRES:EGFP (Vector Builder), which encodes human PDGFB along with transposase-recognized sequences. Control organoids were electroporated with a 1:1 mixture of pRP-CAG-hyPBase and pPB-CAG-EGFP (Vector Builder). After electroporation, organoids were maintained overnight without agitation. On the following day, the medium was replaced with fresh medium, and the organoids were transferred to agitation conditions for long-term culture.

3.6 Immunofluorescence staining

3.6.1 Immunofluorescence staining on cells

mHGG, NPC and mESC were seeded onto glass coverslips pre-coated with Matrigel (BD Biosciences) and fixed with 4% paraformaldehyde (PFA) at room temperature for 15 minutes. Following fixation, cells were washed three times with PBS and permeabilized with PBS 0.5% triton-X for 30 minutes. Non-specific antibody binding sites were blocked with PBS containing 10% normal goat serum (NGS) for 30 minutes. Primary antibody staining was then performed for 2 hours at room temperature in PBS 10% NGS and 0.5% triton-X. Subsequently, secondary antibodies were added for 45 minutes under the same conditions, simultaneously with nuclear staining using Hoechst-33342 dye (1 μg/ml, Sigma-Aldrich).

Primary antibodies used were the following: mouse monoclonal antibodies against Nestin (BD Pharmigen, 556309, 1:250), NeuN (Chemicon, MAB377, 1:100), GFAP (Sigma-Aldrich, G3893, 1:200), beta-tubulin 3 (Sigma-Aldrich, T8660, 1:100), Oct3/4 (Santa Cruz, sc-5279, 1:200);

rabbit polyclonal antibodies against Sox2 (AbCam, 97959, 1:500), Pax6 (Covence, PRB.278P, 1:200), Olig2 (Millipore, AB9610, 1:500), NG2 (Chemicon, AB5320, 1:200).

Secondary antibodies used were the following: Alexa Fluor 488-conjugated AffiniPure anti-mouse IgG (H+L) (Jackson Immunoresearch Laboratories, 115-545-166, 1:500), Dylight 549-conjugated AffiniPure anti-rabbit IgG (H+L) (Jackson Immunoresearch Laboratories, 111-505-003, 1:500).

3.6.2 Immunofluorescence staining on sections

Organoids were fixed in 4% PFA overnight at 4°C, cryoprotected in 30% sucrose, included in O.C.T Compound (Bio-Optica) and sectioned on CM3050S cryostat (Leica) producing 10 μm thick cryosections. Sections were stained with the following primary antibodies in PBS 10% NGS 0.5% triton-X: mouse monoclonal antibodies against Nestin (BD Pharmigen, 556309, 1:250), NeuN (Chemicon, MAB377, 1:100), GFAP (Sigma-Aldrich, G3893, 1:200), beta-tubulin 3 (Sigma-Aldrich, T8660, 1:100), GLAST (Miltenyi, 130-095-814, 1:50), Map2 (Sigma Aldrich, M4403, 1:500); rabbit polyclonal antibodies against Sox2 (AbCam, 97959, 1:500), Pax6 (Covence, PRB.278P, 1:200), Olig2 (Millipore, AB9610, 1:500), ki67 (AbCam, ab15580, 1:100), Sox2 (Merck, 28826070, 1:1000); chicken polyclonal antibodies againt GFP (AbCam, 13970, 1:500), GFP (Aves Labs, GFP-1020, 1:500); rat monoclonal antibodies against CD140a (PDGFRalpha, BD Pharmigen, 558774, 1:100), Ki67 (Thermo Fisher Scientific, 14-5698-82, 1:300); guineapig monoclonal antibodies against Iba1 (Synaptic Systems, 234 308, 1:1000), DCX (Merck, AB2253, 1:1000).

Sections were stained with the following secondary antibodies in the same conditions, simultaneously simultaneously with nuclear staining using Hoechst-33342 dye (1 μg/ml, Sigma-Aldrich): Alexa Fluor 488-conjugated AffiniPure anti-mouse IgG (H+L) (Jackson Immunoresearch Laboratories, 115-545-166, 1:500), Dylight 549-conjugated AffiniPure anti-rabbit IgG (H+L) (Jackson Immunoresearch Laboratories, 111-505-003, 1:500), Alexa Fluor 488 anti-chicken IgG (H+L) (Molecular Probes, A11039, 1:500), Alexa Fluor 660 goat IgG (H+L) anti-rabbit (Life Technologies, A21074, 1:500).

Apoptotic nuclei were revealed using In Situ Cell Death Detection Kit TMR red (Roche) following the instruction of the manufacturer.

3.7 Gaussia Luciferase assay

Gluc activity was evaluated weekly in a reaction set up obtained by combining 5 μl of media conditioned by Gluc-expressing mHGG or neural organoids co-cultured with Gluc-expressing cells with 25 μl of buffer constituted by 1:100 Renilla Luciferase Assay Substrate and Renilla Luciferase Assay Buffer from the Renilla Luciferase Assay System (Promega). The luminometer (Promega Glomax 20/20n) was set to acquire a series of 40 consecutive measures with an integration time of 1 second.

3.8 Animal procedures

All animal procedures were approved by the internal committee for the protection of animals used for scientific purposes (OPBA) of the IRCCS Ospedale Policlinico San Martino and by the Italian Ministry of Health according to the italial law D. lgs 26/2014 and the European Directive 2010/63/EU of the European Parliament. All experiments were performed on C57BL/6 mice.

In utero intraventricular injections of replication-incompetent retroviral vectors were performed on deeply anesthetized pregnant dams at the fourteenth day of gestation. Following laparotomy, uterine horns were exposed, and embryos were injected within the telencephalic ventricles with approximately 2 µl of retroviral suspension containing 1% polybrene (Sigma) to facilitate cell infection. After birth, injected animals were monitored daily and sacrificed when a tumor mass was detected in nuclear magnetic resonance (NMR) around day 40, or anyway at the appearance of neurologic symptoms.

The NMR exam has been performed with a 7 Tesla Bruker BioSpin MRI GmbH (Ettlingen, Germania). The system is equipped with Paravision 360 software and dedicated surface coils for mouse brain imaging. During magnetic resonance images acquisition, mice were anesthetized with isoflurane in O_2 at 2–2.5% for induction and maintained at 1–1.5%. Body temperature was maintained between 35°C and 37°C using a heated animal bed, and respiratory rate was continuously monitored and kept within 80-120 breaths per minute by adjusting the anesthetic concentration. The imaging protocol included the use of a phased-array coil for the mouse brain, and T2-weighted turboRARE sequences were acquired.

Tumor masses were visualized by using a Leica fluorescence microscope thanks to the EGFP expression and dissected in HBSS medium (Life Technologies). Tumor cells were dissociated with enzymatic digestion in Trypsin/EDTA and mechanical dissociation with a Pasteur pipette in 10% FBS (Life Technologies) and after centrifugation at 500xg for 5 minutes, the pellet was resuspended in debris removal solution (Miltenyi Biotec) and debris were removed following the manufacturer instructions. Briefly, the debris removal solution containing tumor cells was overlayed with PBS and centrifuged for 10 minutes at 3000xg at 4°C. Then, the buffer and the interphase containing the cell debris are removed and the pellet is washed with PBS. After a centrifugation for 10 minutes at 1000xg at 4°C, the pellet was resuspended in PBS supplemented with 1% FBS and 1.5 mM EDTA for fluorescent activated cell sorting (FACS).

3.9 Flow cytometry

Tumor cell sorting was perfoemed on a FACSAria II (BD Biosciences) with a 85 µm nozzle tip at a default pressure of 45 psi with the highest precision sort mode. Discrimination doublets and checked sorting gate were done with a dot plot where GFP-Area parameter matched with GFP-Width parameter and then monitored in a FSC-A vs SSC-A dot plot. Sorted GFP+ tumor cells were resuspended in DMEM/F12 medium (Thermo Fisher Scientific) supplemented with 1:50 B27 (Thermo Fisher Scientific), 10 ng/ml recombinant human FGF2 (PreproTech), 10 ng/ml recombinant human EGF (PreproTech) and Penicillin-Streptomicin (Thermo Fisher Scientific),

and they were seeded on neural organoids (5000 or 30.000 cells per organoid, depending on experimental group).

3.10 Image analysis

Image analyses were performed using ImageJ software. For the quantification of cells positive for nuclear markers (Sox2, Oct3/4, Ki67, TUNEL), fluorescent signal was measured in the relevant channel within a region of interest (ROI) automatically defined based on nuclear staining (Hoechst). For the quantification of the distance of tumor cells from the edge of the organoid, an custom analisis pipeline was implemented in ImageJ. This approach involved first defining the perimeter of the organoid as a ROI, followed by the identification of individual tumor cell ROIs based on GFP fluorescence. For each GFP+ ROI, the minimum distance to the organoid perimeter was calculated.

3.11 Statistical analysis

Sample sizes for each experiment are indicated in the results sections. Statistical analyses were performed with two-sided t-test when between two conditions and with anova when between multiple conditions.

4 Results

4.1 Mouse neural organoid generation and characterization

Our aim was to establish an in vitro model that recapitulated our in vivo model to study gliomagenesis and glioma progression. Therefore, we generated mouse neural organoids (mNO) from embryonic stem cells. In the following sections, we described the protocol optimization, morphological and cellular characterization of mNO, their use as recipients for mHGG cell transplantation, as well as their genetic modification to model glioma growth and progression in vitro.

4.1.1 Optimization of mouse neural organoid protocol

For the generation of mouse neural organoids (mNO), we opted for an unguided approach, involving the spontaneous self-assembly of mouse embryonic stem cells (mESC) into a structure that contains different brain regions. mESC line E14Tg2A (passages 25–38) was courtesy given by Professor Federico Cremisi (Scuola Normale Superiore, Università di Pisa) and their pluripotency was assessed through immunostaining for pluripotency markers Oct3/4 and Sox2. Results indicated that 71-98% of cells were positive for Sox2, while 78-93% were positive for Oct3/4, confirming the pluripotent state of the mESCs [Figure 2a].

For the generation of mNO, we adapted a well-established protocol originally designed for human neural organoids by Lancaster and Knoblich[69,70]. Briefly, the protocol had four phases, as detailed in the methods section (Mouse neural organoids): 1) embryoid body (EB) formation; 2) neural induction; 3) static differentiation; 4) dynamic differentiation [Figure 2b]. The optimization was about the EB formation step and the passage between neural induction and static differentiation. Regarding the EB formation phase, the original protocol for human neural organoids used a media suitable for human iPSC and little information was present in the literature regarding a media to use in this phase for mNO. Therefore, we investigated three different media compositions, as detailed in Table 1 and summarized in Figure 2c. Both medium #1 and #2 are commonly employed for the culture of murine embryonic stem cells (mESCs). They share the leukemia inhibitory factor (LIF), a cytokine known for its differentiation-inhibiting properties. However, they diverge in two significant aspects: (1) the absence of fetal bovine serum (FBS) in 2i medium, which eliminates a potential trigger for differentiation; (2) the presence of glycogen synthase kinase 3 (GSK-3) inhibitor CHIR99021 and mitogen-activated protein kinase (MAPK)/extracellular-signal-regulated kinase (ERK) kinase (MEK) inhibitor PD0325901, both playing pivotal roles in maintaining pluripotency in stem cells[127]. In contrast, medium #3 has primarily served as a differentiation medium in guided cortical organoid studies[128,129].

On day 0, mESC cells were plated in an ultra-low attachment 96 well plate either in medium #1 (n=12), medium #2 (n=48) or medium #3 (n=48), and the correct differentiation of mNO was observed over the following 15 days, according to the hallmarks given in the literature[70]. On day 6, EBs were transferred into neural induction medium. At this stage, when observed under the microscope, EBs should exhibit increased brightness around their periphery, indicative of

neuroectodermal differentiation. Remarkably, only EBs cultured in medium #1 displayed these distinct brighter regions, which gradually began to exhibit a radial organization, resembling a pseudostratified epithelium. EBs cultured in medium #3 also showed increased brightness around the periphery but lacked the radial organization seen in the medium #1 group. In contrast, EBs cultured in medium #2 did not exhibit any optically translucent, radially organized neuroectoderm. On day 11, organoids ended the neural induction and were embedded in Matrigel droplets. During the differentiation stage, organoids were expected to form buds of more expanded neuroepithelium. Organoids cultured in medium #1 exhibited the desired morphology. In contrast, organoids cultured in medium #3 and medium #2 failed to develop neuroepithelial buds. Instead, they displayed extended cell processes, indicative of direct neural differentiation [Figure 2d].

Another step that was optimized during protocol refinement was the Matrigel embedding, originally included as a source of extracellular matrix (ECM) to support cellular organization within the organoid[70]. However, this step proved to be time-consuming and introduced potential contamination risks due to the use of non-sterile material. Given previous evidence showing that neural differentiation can occur independently from exogenous ECM supplementation[130], we tested this modification in our system as well [Figure 2e]. Consistent with observations by Costa and colleagues, we found that organoids cultured without Matrigel exhibited evident tissue budding at later stages compared to the organoids cultured with Matrigel [Figure 2f, black arrows].. Importantly, this slower morphological development did not impact long-term differentiation. At later stages, both conditions led to comparable tissue architecture and neuronal maturation, confirming that the initial ECM, whether exogenously provided or endogenously produced, is not critical for the overall differentiation outcome[130].

	Medium #1	**Medium #2**	**Medium #3**
Basal medium	GMEM	GMEM	GMEM
Serum or supplements	B27 supplement without vit.A 1:50	FBS 10%	FBS 10%
	N2 supplement 1:100		
Small molecules (inhibitors and cytokines)	LIF 10000U/mL	LIF 10000U/mL	SB431542 (TGFb inhibitor) 10μM
	PD0325901 (MEK inhibitor) 1μM		
	CHIR99021 (GSK-3 inhibitor) 3μM		
Constant medium components	L-Glutamine 2mM	L-Glutamine 2mM	L-Glutamine 2mM
	Sodium Pyruvate 1mM	Sodium Pyruvate 1mM	Sodium Pyruvate 1mM
	MEM-NEAA 0,1mM	MEM-NEAA 1mM	MEM-NEAA 0,1mM
	β-mercaptoethanol 0,05mM	β-mercaptoethanol 0,05mM	β-mercaptoethanol 0,05mM

Table 1. Detailed composition of the media for EBs formation.

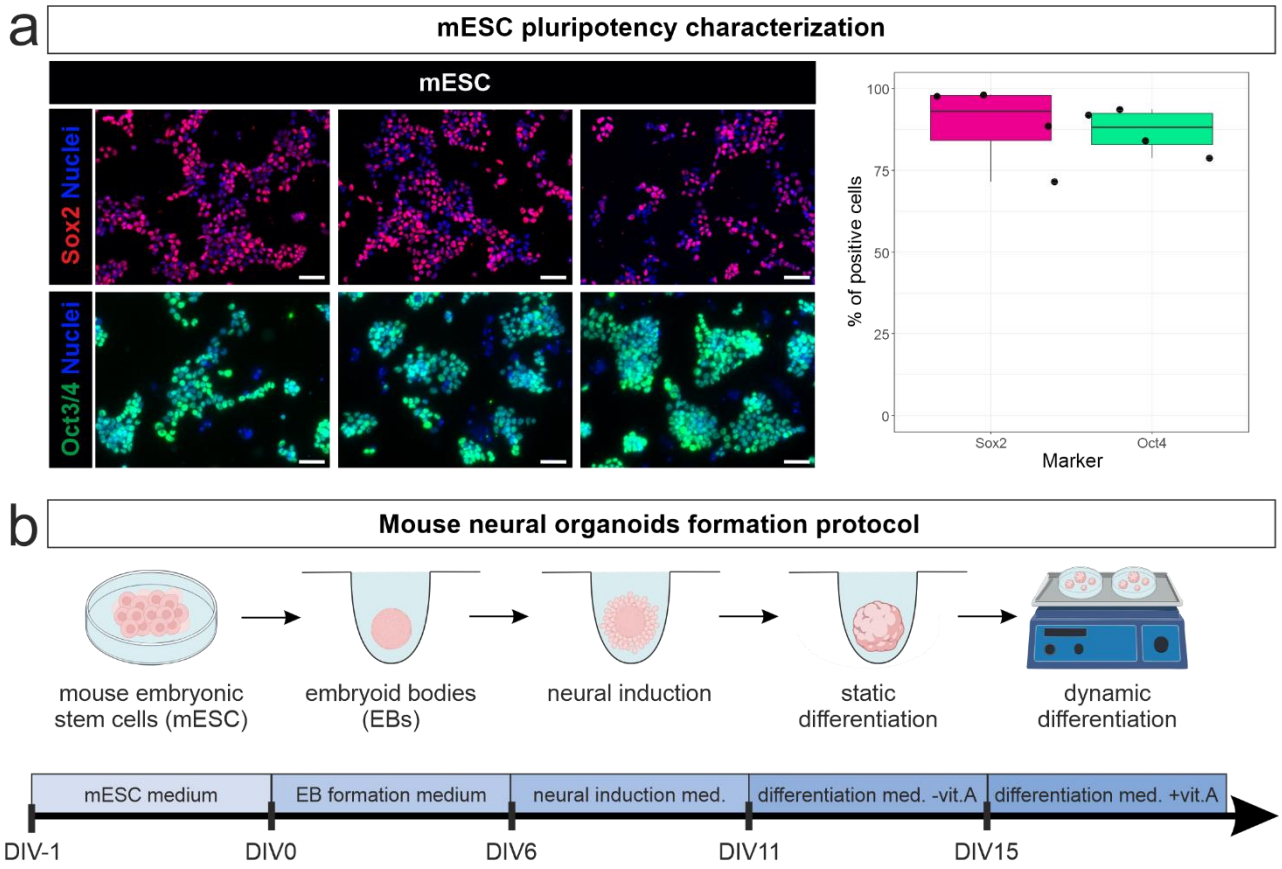
a
mESC pluripotency characterization
mESC
Sox2 Nuclei
Oct3/4 Nuclei
% of positive cells
100
75
50
25
0
Sox2
Oct4
Marker
b
Mouse neural organoids formation protocol
mouse embryonic stem cells (mESC)
embryoid bodies (EBs)
neural induction
static differentiation
dynamic differentiation
mESC medium
EB formation medium
neural induction med.
differentiation med. -vit.A
differentiation med. +vit.A
DIV-1
DIV0
DIV6
DIV11
DIV15
c
EB media composition
#1
#2
#3
GMEM
FBS
TGFβ inhibitor
B27
N2
LIF
GSK3 inhibitor
MEK inhibitor
d
EB formation
Neural induction
Static differentiation
Dynamic differentiation
#1
#2
#3
e
Static differentiation phase
+ Matrigel
neural induction
static differentiation
- Matrigel
neural induction
static differentiation
f
EB formation
Neural induction
Static differentiation
Dynamic differentiation
+ Matrigel
- Matrigel

Figure 2. Optimization of a mouse neural organoid (mNO) protocol. (**a**) Immunofluorescence analysis confirmed the pluripotency of the E14Tg2A mESC line, with high expression of Sox2 (red) and Oct3/4 (green). Nuclei were counterstained with Hoechst (blue) Scale bars = 50 μm. Boxplot represented the quantification of nuclei positive for the pluripotency markers. (**b**) Schematic representation of the four-step protocol used to generate mNOs: embryoid body (EB) formation, neural induction, static differentiation, and dynamic differentiation. (**c**) Composition of the three media tested for the EB formation step. Media #1 and #2 supported pluripotency via LIF, while medium #3 was typically used for differentiation. (**d**) Brightfield images showing morphological differences during organoid development across the three media. Only EBs generated in medium #1 displayed neuroepithelial features, such as translucent peripheral zones and radial organization (white arrowheads), and progressed to form neuroepithelial buds (black arrows). Scale bars = 200 μm. (**e**) Scheme comparing organoids embedded in Matrigel versus cultured without ECM addition during static differentiation. (**f**) Organoids cultured with or without Matrigel exhibited neural tissue budding (black arrows). In the presence of Matrigel-derived ECM, tissue budding occurred earlier during the static differentiation phase, while in its absence, budding became evident only later during dynamic differentiation. Scale bars = 200 μm.

4.1.2 Morphological characterization of mouse neural organoids

To evaluate the cellular composition and structural organization, we performed immunofluorescence staining on 30-day-old mNO using markers specific to key neural and glial cell types. Neural progenitor cells (NPCs) were identified by the expression of Sox2 and Nestin, indicating the presence of undifferentiated neural precursors. In addition, radial glial (RG) cells were detected through the co-expression of Sox2 and GLAST [Figure 3a]. Sox2+ cells were frequently organized in rosette-like structures, characterized by radial organization around a central lumen and reminiscent of the neuroepithelial organization found in the early developing neural tube [Figure 3b]. These structures represent an in vitro correlation of ventricular zones and their presence within the mNO confirms the establishment of spatially organized progenitor domain. Post-mitotic neurons, marked by NeuN, were observed alongside proliferating Ki67+ cells, indicating ongoing neurogenesis. Early neuronal processes were visualized by βIII-tubulin (TubbIII) staining [Figure 3c]. Despite the original protocol the presence of glial cells was not investigated[70], we investigated their presence as well because we thought that their presence was relevant to the generation of an in vitro environment that was more reminiscent of a brain. Both astrocytes, identified by GFAP expression, and mature oligodendrocytes, identified via Olig2 staining, were present. However, oligodendrocytes were scares, as expected by an unguided protocol that did not include any specific differentiating and trophic factor for this lineage. As for astrocytes, they are localized in specific regions of the organoid. [Figure 3d]. This diversity suggests that, by day 30, the organoids had already established a complex neural environment containing both neuronal and glial populations.

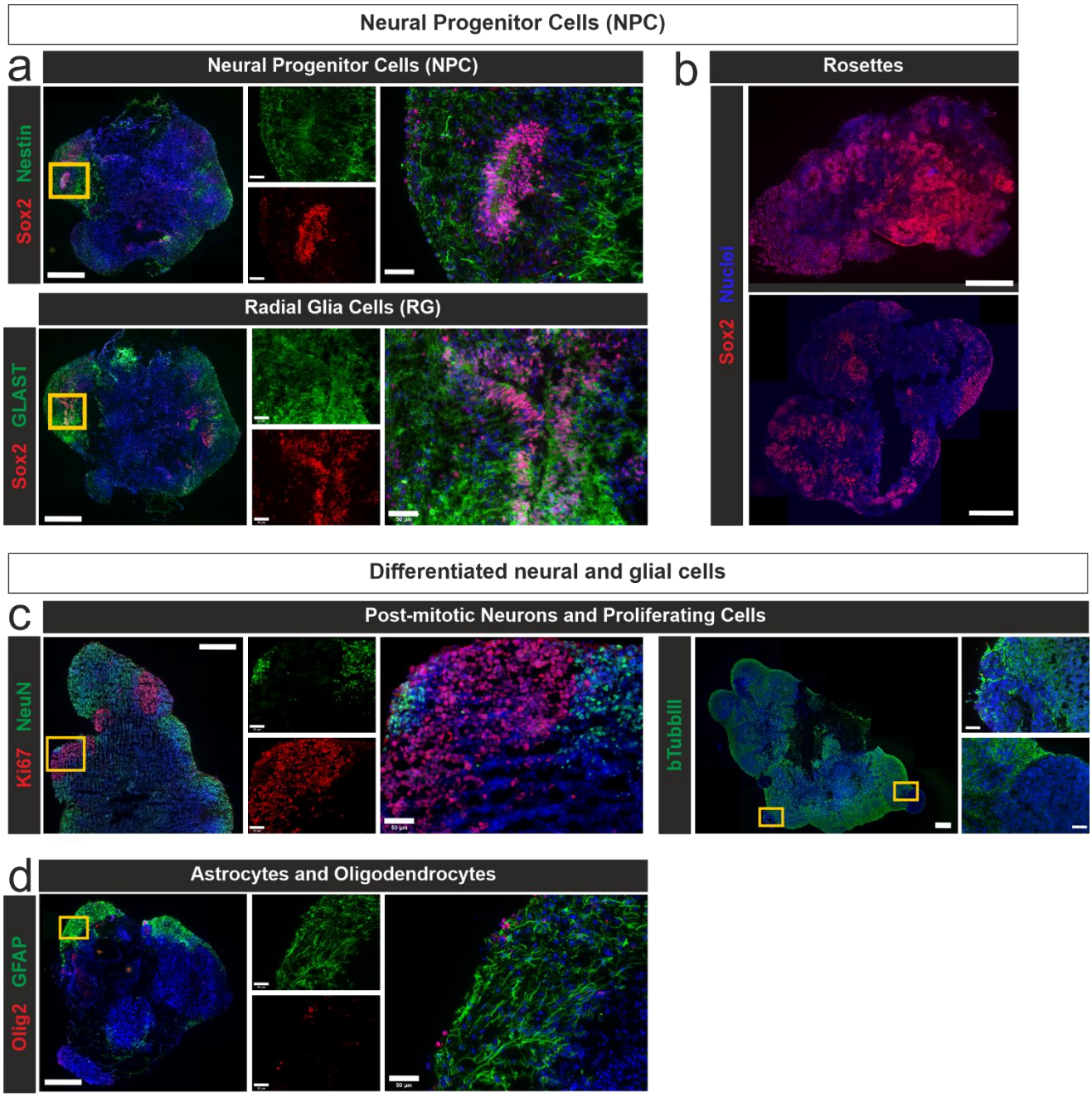

Figure 3. Immunofluorescence-based characterization of 30-day-old neural organoids. (**a**) Neural progenitor cells (NPCs) were identified by co-expression of Sox2 (red) and Nestin (green), while radial glia (RG) cells expressed Sox2 (red) and GLAST (green). Close ups show high-magnification views of selected regions (yellow boxes). (**b**) Sox2+ cells organized into rosette-like structures, recapitulating early neuroepithelial architecture. Nuclei are stained with Hoechst (blue). (**c**) Post-mitotic neurons (NeuN, green) and proliferating cells (Ki67, red) co-exist within the organoid tissue. Immature neurons and developing processes were also detected by βIII-tubulin (TubbIII, green). (**d**) Glial populations were detected, including GFAP+ astrocytes (green) and Olig2+ oligodendrocyte lineage cells (red). All images correspond to 30-day-old organoids. Nuclei are counterstained with Hoechst (blue). Scale bars: 500 μm for the mosaic images and 50 μm for the close ups.

4.1.3 Mouse neural organoid derivation from neural precursor cells

To streamline the generation of mouse brain organoids, we employed mouse neural progenitor cells (NPCs) isolated from embryonic day 14.5 (E14.5) embryos and cultured in B27-supplemented medium (referred to as B27c medium). Immunostaining demonstrated that NPCs exhibited characteristic neural progenitor markers, including Sox2 and Nestin, along with the unexpected expression of Olig2, a marker typically associated with oligodendrocytes. Conversely, they did not express markers indicative of more differentiated cell types, such as NeuN and β-tubulin III [Figure 4a]. Given their pre-committed neural identity, we initially tried to bypass the neural induction step. NPC seeded in ULA 96-well plate formed spheroids within 4 days (n=16). However, upon embedding in Matrigel, all organoids displayed elongated cellular processes within the matrix, without the formation of organized neuroepithelial structures, indicating failed organoid architecture according to the procotol used for mESC [Figure 4b]. hypothesized that this aberrant differentiation could be driven by B27c medium, which may promote premature differentiation, as evidenced by the expression of Olig2. To test this, NPC cultures were transitioned to one of the media used for mESC (referred to as ES medium). Under these conditions, a reduction in nuclear Olig2 expression was noted, with the protein being largely localized in the cytoplasm, while Sox2 expression was retained [Figure 4c-d]. This observation suggested that NPC cultures in ES medium retained certain pluripotent features while modulating the nuclear presence of a transcription factor associated with mature cell types. Based on this, we attempted to generate mouse brain organoids using NPC cultures in ES medium. However, two major limitations emerged: (1) NPCs failed to efficiently aggregate into spheroids, and (2) in cases where aggregation occurred, spheroids stopped growing [Figure 4e]. It is possible that, unlike mESC-derived aggregates, the presence of cellular processes in this context did not reflect aberrant differentiation but rather an intrinsic behavior of NPCs following aggregation. Nonetheless, when spheroids were transferred to differentiation medium supplemented with vitamin A, growth arrest was observed, likely due to incompatibility between the standard culture conditions required for NPC maintenance and the media used in the organoid differentiation protocol. Together, these results indicate that NPC maintained in either B27c or ES medium are not a suitable starting material for mouse brain organoid generation using this protocol.

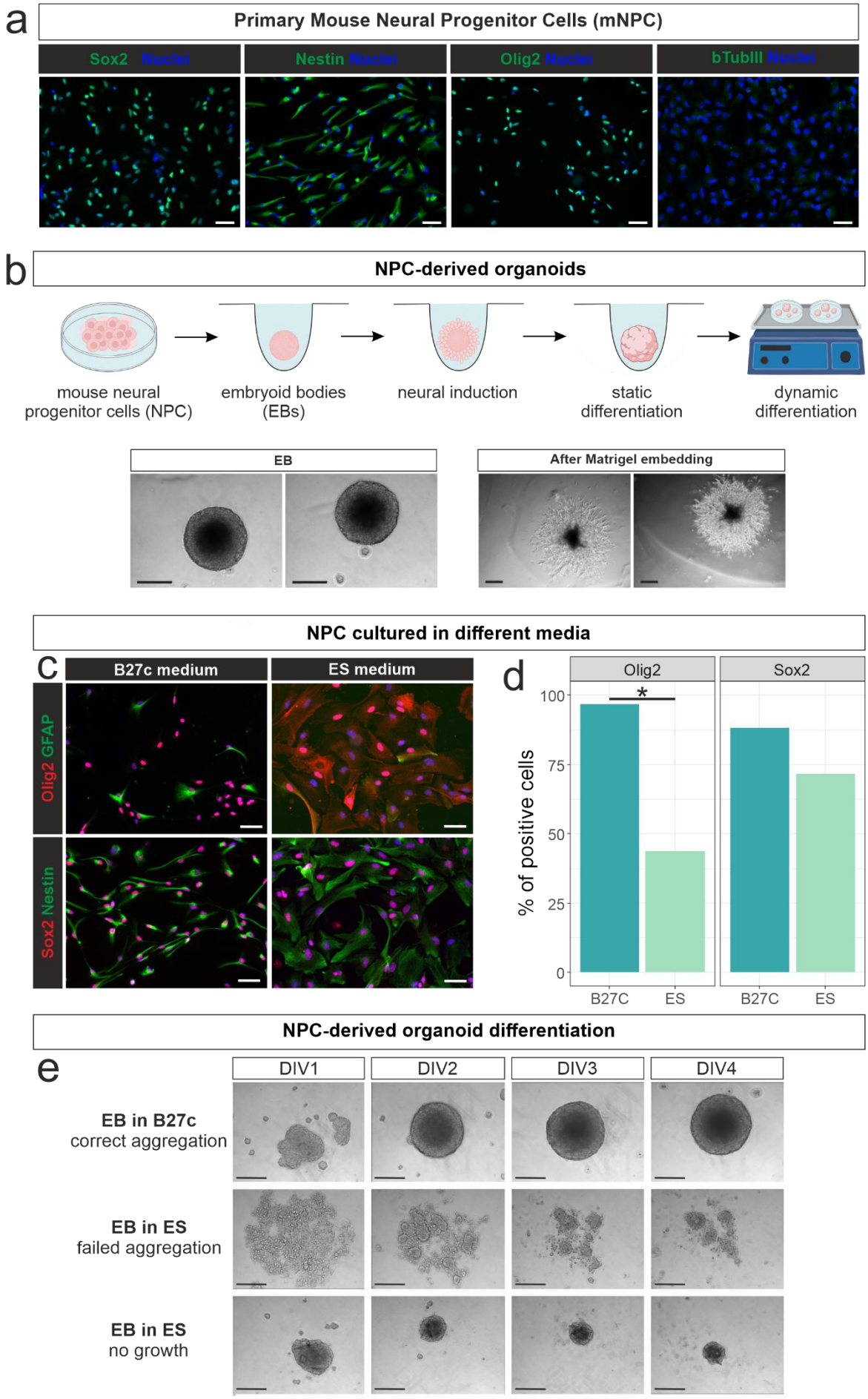
a
Primary Mouse Neural Progenitor Cells (mNPC)
Sox2 Nuclei
Nestin Nuclei
Olig2 Nuclei
bTubIII Nuclei
b
NPC-derived organoids
mouse neural progenitor cells (NPC)
embryoid bodies (EBs)
neural induction
static differentiation
dynamic differentiation
EB
After Matrigel embedding
NPC cultured in different media
c
B27c medium
ES medium
Olig2 GFAP
Sox2 Nestin
d
Olig2
Sox2
% of positive cells
100
75
50
25
0
*
B27C
ES
B27C
ES
NPC-derived organoid differentiation
e
DIV1
DIV2
DIV3
DIV4
EB in B27c
correct aggregation
EB in ES
failed aggregation
EB in ES
no growth

Figure 4. Evaluation of mouse neural progenitor cells (NPCs) as starting material for brain organoid generation. (**a**) Immunofluorescence analysis of primary mouse NPCs confirmed the expression of Sox2, Nestin and Olig2 and the non-expression of βtubulin III. Scale bars= 50 μm.(**b**) Schematic and brightfield images showing organoid generation from NPCs: although embryoid bodies (EBs) formed, Matrigel embedding resulted in elongated cellular projections without organized neuroepithelium. Scale bars: 200 μm. (**c**) Immunostaining comparison of NPCs maintained in B27c versus ES medium. In ES medium, nuclear Olig2 expression is reduced while Sox2 is retained. Scale bars: 50 μm.(**d**) Quantification of Olig2 and Sox2-positive nuclei confirmed the reduced expression of nuclear Olig2 in ES medium, while Sox2 expression is comparable in the two culture conditions. * p-value < 0.05 (**e**) Brightfield time-course of EB formation and growth in B27c and ES media. NPCs in ES failed to aggregate or grow properly, indicating unsuitability for organoid generation. Scale bars: 200 μm.

4.2 Glioma generation and characterization in mouse neural organoids

Once we established a suitable mNO containing all the relevant cell types, we focused on the development of in vitro glioma model using these organoids as a platform. In particular, we explored two complementary approaches:

1) A cell-based approach, that involved the inoculation of primary murine glioma cells (either high-grade or low-grade) in mNO through co-culture or direct transplantation, allowing tumor cells to grow within the organoid environment.
2) A genetic-based approach, that relied on the genetic modification of healthy cells in mNO to induce malignant transformation and tumor formation.

The cell-based approach is valuable in modelling tumors derived from patient samples, as it preserves the intrinsic features of primary glioma cells in an environment that is more similar to a brain than the plastic. In contrast, the genetic-based approach is better suited for investigating gliomagenesis and early molecular and cellular events that drive glioma initiation and progression.

4.2.1 Co-culture of glioma cells with mNO

We chose to begin with the co-culture approach because it was technically more feasible and time-efficient compared to genetic engineering approaches, requiring fewer steps and less optimization. Moreover, tumor cells were already available in the laboratory. By starting with this strategy, we could quickly assess the compatibility between mNO and glioma cells before moving on to the more complex and time-consuming genetic-based modeling.

4.2.1.1 Optimization of the co-culture method

To identify the optimal strategy for incorporating tumor cells into mNO, we evaluated three co-culture methods [Figure 5a]:

1) Co-culture of tumor cells and organoids in a 24-well plate, followed by transfer to a new 24-well plate in agitation.
2) Co-culture of tumor cells and organoids in 96-well plate, followed by transfer to petri dish in agitation.
3) Fusion of pre-formed tumor spheroids with organoids in 96-well plate, followed by transfer to petri dish in agitation.

Among these, protocol #2 demonstrated consistent tumor cell integration and extensive infiltration, as shown by immunofluorescence imaging identifying GFP+ tumor cells throughout the organoid tissue. In contrast, protocol #1 and #3 resulted in limited or superficial integration

[Figure 5b]. Quantification of tumor cells in sections confirmed a significantly higher tumor cell counts in organoids from protocol #2 compared to protocol #1 ($p<0.05$) and protocol #3 ($p<0.01$) [Figure 5c]. As for the quantification of the tumor cell invasiveness into the organoid parenchyma, no significant differences were observed among the three protocols [Figure 5d]. However, there was a trend toward reduced invasiveness in protocol #1, suggesting a less efficient penetration of tumor cells. Moreover, protocol #2 also proved to be the most practical and time efficient. In contrast, protocol #1 required the use of 24-well plates, which not only led to a more dispersed distribution of tumor cells—reducing their chances of successfully attaching to the organoids—but also made routine maintenance, such as media changes, more labor-intensive. On the other hand, protocol #3 required an additional step for the generation of tumor spheroids and a longer incubation period (48 hours versus 24 hours for protocols #1 and #2), making it more time-consuming. Based on both efficacy and practicality, protocol #2 was selected as the standard protocol for subsequent glioma-mNO co-culture experiments.

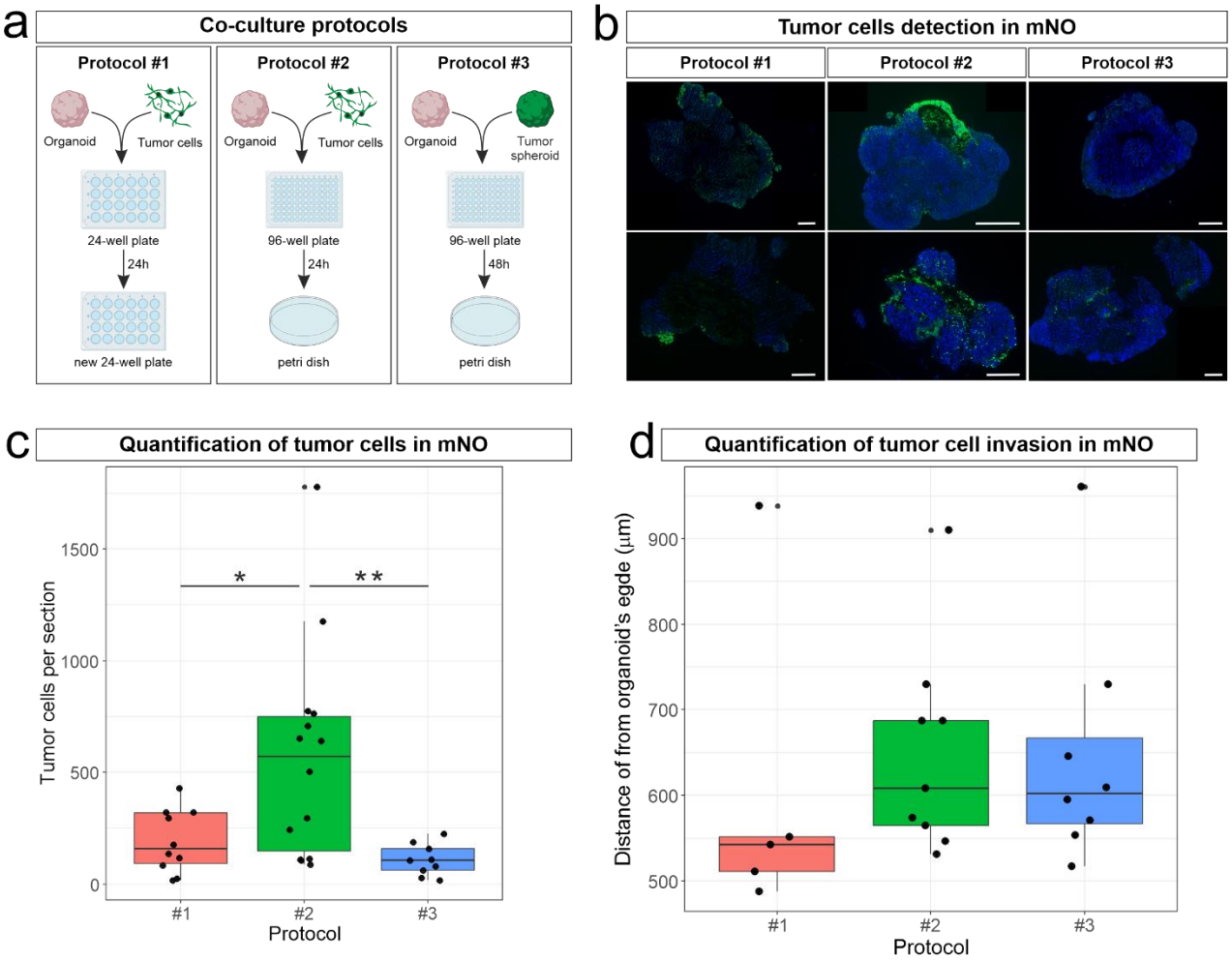

Figure 5. Comparison of glioma cell integration methods into mouse neural organoids. (**a**) Scheme of the three protocols tested: co-culture in 24-well plate with subsequent transfer to a new 24-well plate under agitation (Protocol #1), co-culture in 96-well plate with subsequent transfer to petri dish under agitation (Protocol #2), and fusion with tumor spheroids in 96-well ULA plates with transfer to petri dish under agitation after 48h(Protocol #3). (**b**) Representative immunofluorescence images of GFP+ tumor cells (green) integrated within mNO (nuclei stained blue). Protocol #2 shows widespread infiltration of tumor cells, whereas Protocol #1 and #3 show superficial or no integration Scale bars: 500 µm. (**c**) Quantification of infiltrating tumor cells per organoid for each protocol (dots represent sections analyzed). Median cell counts are shown as horizontal bars; error bars indicate range. Protocol 2 yielded significantly more tumor cells compared to Protocol #1 ($p < 0.05$) and Protocol #3 ($p < 0.01$). (**d**) Quantification of the median distance of the most invasive (nineteenth percentile) GFP+ tumor cells in each section.

4.2.1.2 Mouse neural organoids support maintenance and invasive capacity of high-grade glioma cells

To evaluate the capacity of mouse neural organoids (mNO) to support the maintenance of tumor cells, we first established tumor-bearing brain organoids by co-culturing them with two primary mouse high-grade glioma cells (mHGG#1 and mHGG#2). Organoids were collected and analyzed at 10, 20, 30 and 40 days post co-culture [Figure 6a]. GFP+ tumor cells were visible under the microscope a few days after the start of the co-culture, indicating successful engraftment [Figure 6b]. The tumor take rate was high, with 95% of organoids showing the presence of mHGG#1 (103 out of 108 mNO analyzed) and 97% of mHGG#2 (36 out of 37 mNO analyzed). Immunofluorescence analysis on sections of organoids showed changes in the distribution of tumor cells over time, with differences between the two cell lines. As for mHGG#1, tumor cells were predominantly localized at the periphery of the organoid, forming tumor mass-like aggregates, especially at early time points (10 and 20 days). Over time, infiltrating mHGG cells were also observed, as expected from a high-grade glioma cell line, while the tumor masses-like structures remained relatively localized. In contrast, mHGG#2 showed a more aggressive growth pattern starting as early as 10 days post co-culture, with widespread engrafting of tumor cells to the organoid parenchyma [Figure 6c]. Quantification of the area coverage of GFP+ tumor cells showed that mHGG#2 had a significantly larger area of colonization across all time points compared to mHGG#1. In both cell lines, a progressive decrease in area coverage was observed over time, particularly pronounced in the case of mHGG#2 [Figure 6d]. This reduction may be attributed to the fact that many tumor cells grew on the surface of the organoid rather than deeply invading its inner regions. As the culture progresses, tumor cells superficially attached may detach, a process likely favored by the constant agitation of the culture condition. This is also supported by the fact that GFP+ debris and detached organoid fragments were frequently observed in long-term cultures and typically removed during routine medium changes.

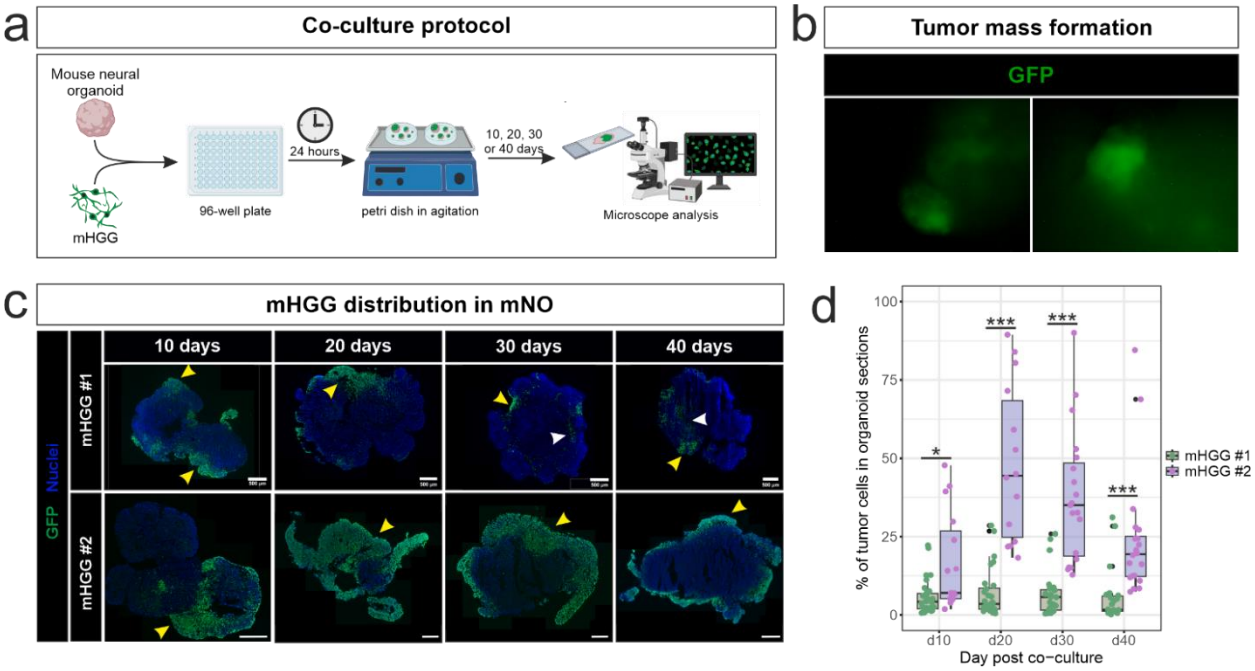

Figure 6. Establishment and longitudinal analysis of glioma-bearing mouse neural organoids (mNO). (**a**) Schematic representation of the experimental workflow: primary mHGG cells (GFP+) were co-cultured with mNO and collected for analysis at multiple time points (10, 20, 30, and 40 days). (**b**) Representative fluorescence images of whole mNO showing GFP+ tumor cells a few days after co-culture, confirming successful engraftment. (**c**) Immunofluorescence analysis of organoid sections at four time points after co-culture with two different mHGG lines (GFP in green; nuclei in blue). mHGG#1 mainly localized at the organoid periphery forming tumor mass-like structures (yellow arrowheads), while mHGG#2 showed a more widespread infiltration within the organoid parenchyma. White arrowheads indicate deeper invasion zones. Scale bar: 500 µm. (**d**) Quantification of the area covered by GFP+ tumor cells in organoid sections co-cultured with mHGG#1 (green) and mHGG#2 (purple) at 10, 20, 30, and 40 days post co-culture. Values are expressed as the percentage of the organoid area occupied by GFP+ cells. Data show significantly greater colonization by mHGG#2 across all time points, indicating a higher infiltrative and proliferative capacity compared to mHGG#1. Each dot represents an individual organoid. Statistical analysis: *p-value < 0.05; t- test, ***p-value < 0.001

The proliferative state of mHGG cells co-cultured with mNO was confirmed by immunostaining for ki67, that is a proliferation marker also used in the clinical setting to gain information on the tumor aggressiveness and therapeutic responsiveness[131,132]. Tumor cells were proliferating across all the time points analyzed, with the median percentage of GFP+/ki67+ cells ranging from 59.0% to 92.4%, without any significant difference between the two tumor cell lines (for mHGG #1, 10 days: 82.4±18.2; 20 days: 59.0±31.0; 30 days: 63.0±15.8; 40 days: 75.8±10.5; for mHGG #2, 10 days: 92.4±9.7; 20 days: 79.7±13.1; 30 days: 77.7±14.5; 40 days: 75.8±13.6) [Figure 7a-c]. Additional confirmation of the proliferative state of mHGG was provided by Sox2 staining: Sox2+ tumor cells were consistently detected at all time points, with percentages ranging from 52.9% to 87.4%, even in this case without any significant difference between the tumor cell lines (for mHGG #1, 10 days: 79.8±18.9; 20 days: 52.9±19.7; 30 days: 68.5±8.8; 40 days: 70.3±10.9; for mHGG #2, 10 days: 87.4±14.9; 20 days: 85.3±24.9; 30 days: 71.5±18.2; 40 days: 71.3±11.2) [Figure 7b-c]. These findings indicate that the organoid environment supports tumor cell proliferation and the preservation of stem-like features.

To further investigate the tumor cell growth dynamic in mNO over time, we hypothesized that while a portion of tumor cells continued to proliferate, another fraction may undergo cell death. To test this hypothesis, a pilot TUNEL assay was performed on organoid sections. This preliminary analysis revealed that only a small proportion of mHGG cells was apoptotic at each timepoint analyzed, even though a slight increase in the percentage of apoptotic cells was observed by 30 days post co-culture, with the median percentage of GFP+/TUNEL+ cells passing from 5.41% to 11.4% [Figure 7d-e]. Although further validation is necessary, these results are consistent with the proliferation analysis, indicating that while a small percentage of tumor cells was apoptotic, the majority actively proliferated within the organoid microenvironment.

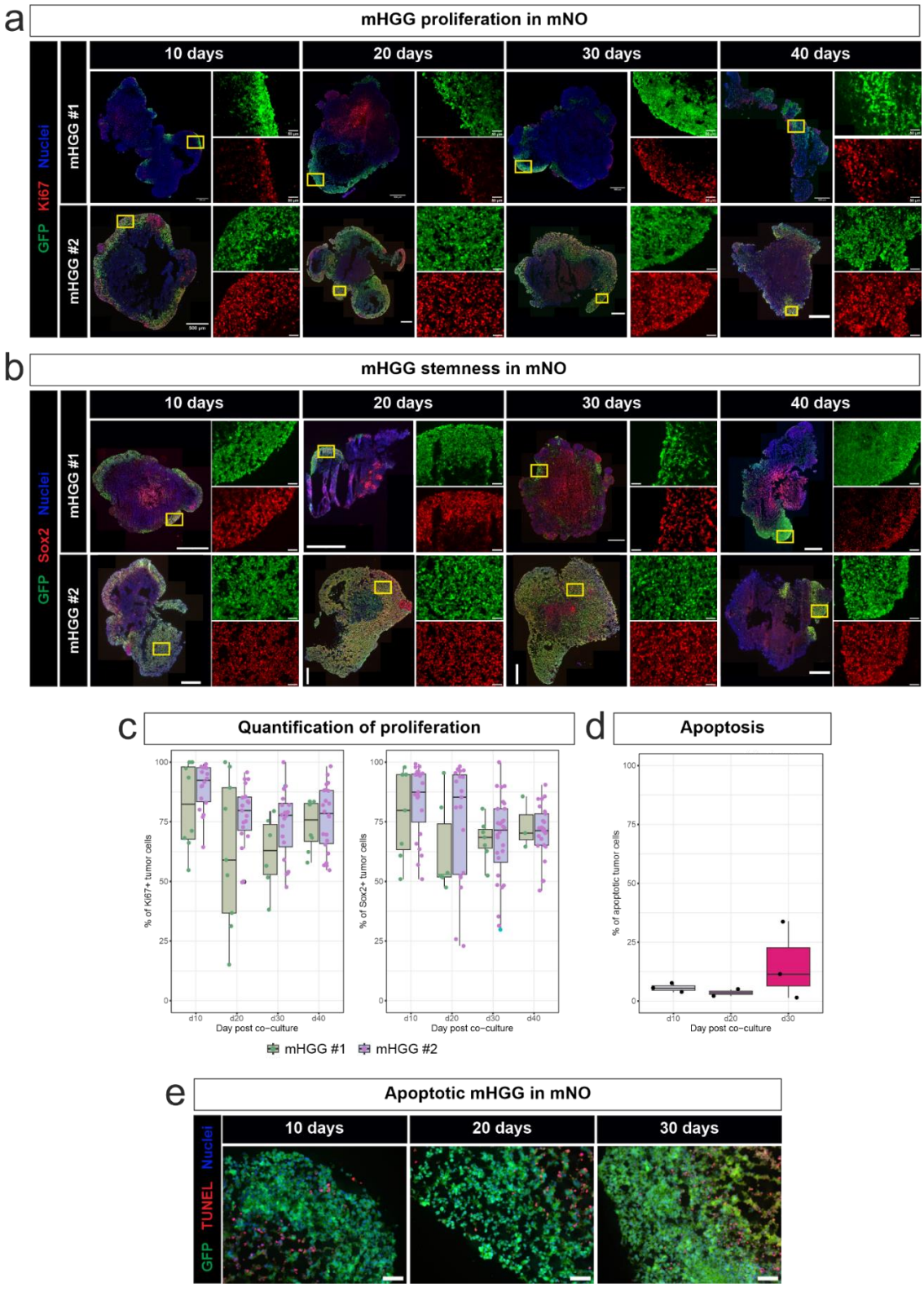

Figure 7. Proliferation and stemness maintenance of mHGG cells in mNO. (**a**) Representative fluorescent images of mNO sections at 10, 20, 30, and 40 days post-co-culture showing mHGG cells (GFP^+) positive for the proliferation marker Ki67 (red). Nuclei are stained in blue. Close ups highlight regions of proliferative activity. Scale bars: 500 µm (overview), 50 µm (insets). (**b**) Immunofluorescence staining for Sox2 (red) in mHGG cells (GFP^+, green) at the same time points, indicating maintenance of stemness. (**c**) Boxplot representing the quantification of the percentage of $Ki67^+$ (left) and $Sox2^+$ (right) cells among GFP^+ mHGG cells over time. Each point represents an organoid section analyzed. (**d**) Boxplot representing the quantification of apoptotic mHGG cells (GFP+/TUNEL+) at 10, 20, 30, and 40 days, showing a slight increase in apoptosis at 30 days, though not significant. Each point represents an organoid analyzed. (**e**) Higher magnification images showing apoptotic (TUNEL+ in red) tumor cells (GFP+ in green) within mNO at different time points. Scale bars: 50 µm.

To overcome possible limitations related to image-based quantification, we decided to take advantage of a bioluminescence technique previously validated in our laboratory and used to follow the growth of tumor masses in vivo[133]. mHGG cells previously engineered to express Gaussia Luciferase (mHGG-gluc) were co-cultured with mNO and tumor cell engraftment was followed via fluorescent microscopy since tumor cells were also engineered to express DsRed. Fluorescence images in the red channel revealed the presence of DsRed+ tumor cells as early as 7 days after the start of the co-culture in 67% of organoids co-cultured with the mHGG-gLuc-1 cell line and in 36% of those co-cultured with the mHGG-gLuc-2 line. After 14 days, these percentages increased to 87% of organoids positive for mHGG-gLuc-1 and 67% for mHGG-gLuc-2. The DsRed+ tumor cells were organized in tumor masses that grow over time [Figure 8a, yellow arrows], recapitulating the behavior of tumors in vivo.

Before applying the measurement of Gaussia Luciferase to the co-cultures, we first verified the correlation between the number of tumor cells and the luminescence signal. To this end, gLuc expression levels were measured at known concentrations of tumor cells. The results confirmed a correlation between the luminescence signal, measured with a luminometer and expressed in Relative Light Units (RLU), and the number of tumor cells [Figure 8b]. Additionally, the analysis revealed that the two cell lines differ in gLuc expression levels: mHGG-gLuc-2 cells showed higher expression of the protein compared to mHGG-gLuc-1 cells when seeded at the same cell number. Once the correlation between measured kRLU and cell number was established, we used gLuc expression measurements to obtain quantitative data on tumor cell dynamics in the organoid co-cultures. The gLuc signal was measured weekly in the culture medium for both cell lines. mHGG-gLuc-2 cells displayed an increasing trend over time, at least up to 35 days of co-culture, in agreement with the growth of tumor masses observed through fluorescence microscopy. In contrast, the luminescence signal from mHGG-gLuc-1 appeared more stable over time. [Figure 8c]. However, we reasoned that the apparent stability of the luminescence signal in mHGG-gLuc-1 co-cultures might be attributed to its intrinsically lower Gaussia Luciferase expression levels compared to mHGG-gLuc-2. This reduced secretion likely resulted in a weaker overall bioluminescent output, thereby limiting the sensitivity of the measurement and potentially masking changes in tumor growth dynamics.

To validate and further investigate the results obtained through the quantification of Gaussia luciferase signal in the culture medium, the proliferative state of mHGG-gLuc cells was also assessed by immunofluorescence analysis on organoid sections at 40 days from the start of co-culture. As for Ki67 staining, proliferating tumor cells ranged from 58.8% to 68.0% for mHGG-gLuc-1 line and from 52.4% to 66.3% for mHGG-gLuc-2 [Figure 8d]. Similar results were obtained also for Sox2 staining, in which percentages of positive tumor cells were ranging from 78.8% to 88.7% for mHGG-gLuc-1 and from 51.0% to 63.4% for mHGG-gLuc-2 [Figure 8e]. No statistically significant differences between the two cell lines were detected.

The fluorescence and luminescence data showed early engraftment and progressive growth of mHGG cells, particularly in organoids co-cultured with the mHGG-gLuc-2 line. Immunofluorescence analyses confirmed active proliferation and stem-like features in both tumor cell lines, even after 40 days of co-culture.

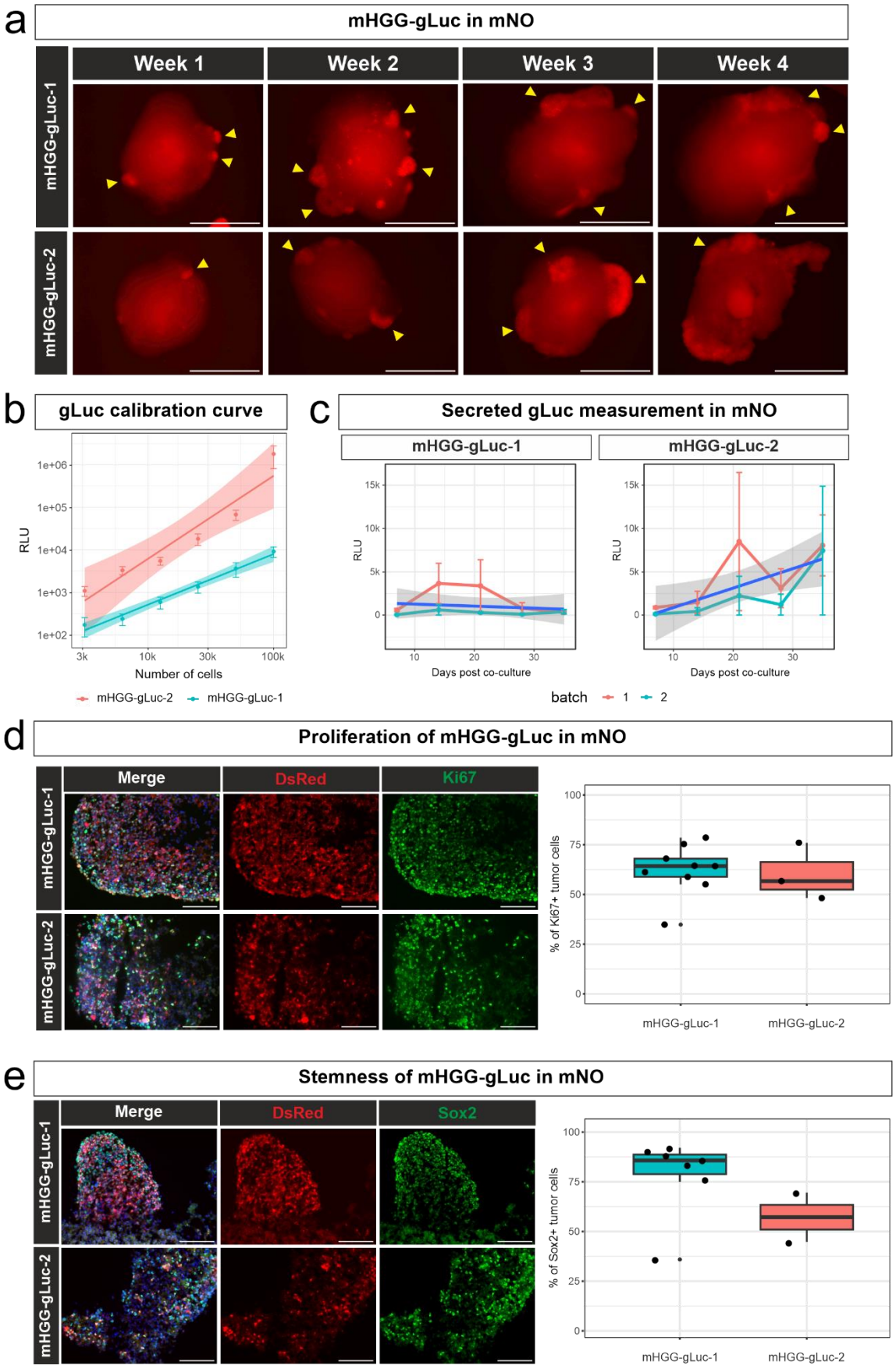

Figure 8. Analysis of proliferation and stem-like features of mHGG cells co-cultured with brain organoids (mNO). (**a**) Fluorescence images in the red channel (DsRed) show the progressive growth of tumor masses in organoids co-cultured with mHGG-gLuc-1 and mHGG-gLuc-2 cell lines from Week 1 to Week 4. Yellow arrows indicate visible tumor masses. (**b**) Calibration curves showing the correlation between Gaussia luciferase (gLuc) signal and tumor cell number for both cell lines. Each point

represents a biological replicate of the experiment, and it is the average of two technical replicates. Error bars represent the standard error of the mean (SEM) (**c**) Weekly monitoring of gLuc expression in the culture medium, expressed as RLU, in mHGG-gLuc-1 (left) and mHGG-gLuc-2 (right) co-cultures. Each dot represents the median signal from one batch and error bars represent the standard deviation. The blue line represents a linear regression, and the grey shaded area indicates the 95% confidence interval. (**d**) On the left, immunofluorescence analysis on organoid sections at 40 days of co-culture. Images show co-localization of DsRed (red) with Ki67 (green). Scale bars = 100 μm. On the right panel, boxplot shows the quantification of the percentage of tumor cells positive for Ki67. (**d**) On the left, immunofluorescence analysis on organoid sections at 40 days of co-culture. Images show co-localization of DsRed (red) with Sox2 (green). Scale bars = 100 μm. On the right panel, boxplot shows the quantification of the percentage of tumor cells positive for Sox2.

4.2.1.3 Co-culture of mouse neural organoids with low-grade glioma cells did not result in tumor formation

Since mNO supported the maintenance of mHGG cells, we investigated whether they could also support mouse low-grade glioma (mLGG) cells. These cells are non-tumorigenic when transplanted into immunocompetent mice and cannot be propagated in standard in vitro culture conditions. To obtain mLGG cells, in utero intraventricular injection of retroviral particles overexpressing PDGFB was performed on pregnant dams at E14. The appropriate timepoint for the isolation of LGG-derived cells was determined by nuclear magnetic resonance. GFP fluorescence was used to identify tumoral regions, revealing multifocal tumor masses in both animals analyzed [Figure 9a]. mLGG cells were co-cultured with mNO using the same method previously described for the mHGG and organoids were analyzed at the same time points. However, GFP+ mLGG cells were not detected in cryosections at any of the timepoints analyzed [Figure 9b], suggesting that mLGG failed to attach to or invade the organoid.

Considering that neuronal electrical activity plays an important role in glioma progression, we hypothesized that it might be a key factor for the maintenance of mLGG cells in mNO. For this reason, mLGG cells were also co-cultured with one-year-old human neural organoids (hNO) derived from wild-type iPSC (wt-hNO) and iPSC derived from an epilepsy patient (ep-hNO), kindly provided by Prof. Silvia Cappello (Ludwig-Maximilian Universitat, Munich). Since the hNO were GFP+, GFP fluorescent signal could not be used to distinguish hNO endogenous cells from mLGG cells. Therefore, we used two Nestin antibodies: one specific for the human isoform (expressed only in hNO), and the other for the mouse isoform (expressed by mLGG cells). No mouse Nestin signal was detected in any of the organoids analyzed, indicating that mLGG cells did not attach to or invade the human neural organoids [Figure 9c].

This failure of mLGG cells to attach to or invade the mNO may be explained by two main factors. First, it could be method-related: the co-culture approach may be suitable for highly invasive tumor cells, such as mHGG, that have already acquired aggressive traits during tumor progression, but less effective for early-stage, low-grade cells with limited proliferative and infiltrative capacity. Second, it could be biology-related: while the microenvironment provided by mNO appears sufficient to sustain the growth and maintenance of already progressed mHGG, it might still lack specific cues necessary to support the survival or further progression of early-stage mLGG cells.

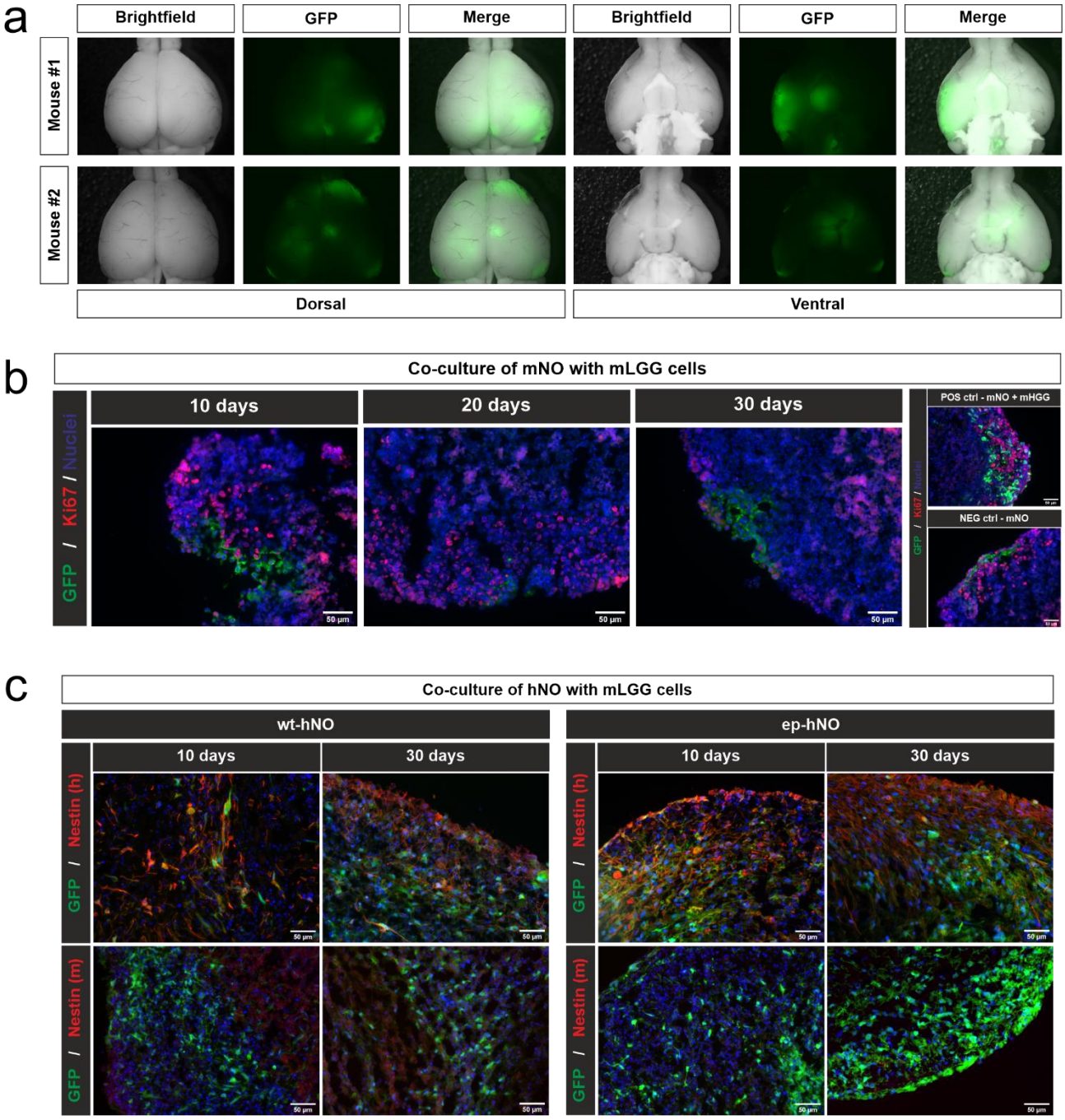

Figure 9. Mouse low-grade glioma (mLGG) cells co-culture with mouse and human neural organoids. (**a**) Representative in vivo GFP fluorescence images of brains from two mice (mLGG#1 and mLGG#2) following in utero intraventricular injection of PDGFB-overexpressing retrovirus at E14, showing multifocal tumor formation. (**b**) Immunofluorescence analysis of mNO co-cultured with GFP+ mLGG cells at 10, 20, and 30 days post co-culture. No persistent GFP signal is detectable at any time point, suggesting failure of mLGG cell engraftment. Ki67 staining (red) highlights host cell proliferation. On the righe panels, positive control (mNO + mHGG) shows clear GFP+ tumor infiltration, while negative control (mNO alone) shows no GFP signal. (**c**) Co-culture of mLGG cells with human neural organoids (wt-hNO and ep-hNO) analyzed at 10 and 30 days. Immunostaining with human- and mouse-specific Nestin antibodies reveals Nestin(h) expression in the organoid, but absence of Nestin(m), indicating that mLGG cells neither attached to nor invaded the hNO, regardless of electrical activity profile

4.2.2 Transplantation of mHGG into mNO

To begin addressing the method-related limitation, we decided to try an alternative strategy for tumor cell delivery that more closely mimics the orthotopic transplantation used in vivo, Specifically, we injected tumor cells directly into mNO, rather than relying on surface co-culture, to facilitate more efficient engraftment and integration.

We first tried this approach with mNO and mHGG. We transplanted 30-day-old mNO with mHGG, kept them in agitation and analyzed them at the microscope every 10 days until 40 days post-transplantation [Figure 10a]. Immunofluorescence staining revealed that mHGG engrafted and expanded within the organoid tissue, maintaining a widespread GFP signal throughout all timepoints [Figure 10b]. Co-staining for Ki67 showed that the majority of tumor cells remained proliferative over time, with quantification indicating from 60.7% to 89.3% of GFP+ cells expressing Ki67 at each timepoint [Figure 10c]. Similarly, Sox2 staining demonstrated that the majority of mHGG cells retained stem-like features post-engraftment, with from 74.6% to 83.0% of GFP+ cells co-expressing Sox2 across the analyzed days [Figure 10d]. These data confirm that mHGG cells can integrate into mNO, where they persist, proliferate, and retain stemness characteristics for at least 40 days post-transplantation. We will apply this method to mLGG to understand whether this could be a more suitable method to mediate their engraftment into mNO.

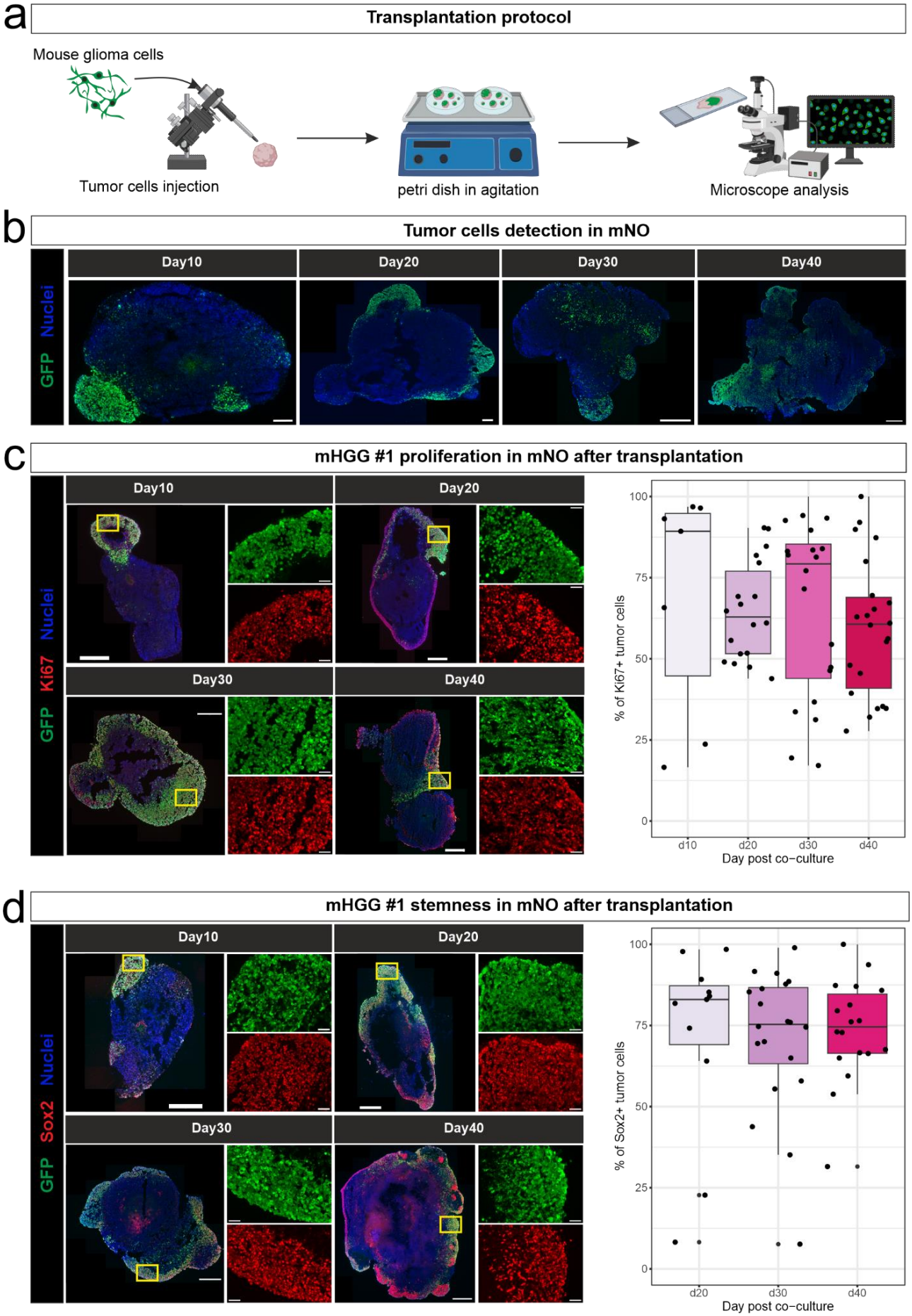
a
Transplantation protocol
Mouse glioma cells
Tumor cells injection
petri dish in agitation
Microscope analysis
b
Tumor cells detection in mNO
Day10
Day20
Day30
Day40
GFP Nuclei
c
mHGG #1 proliferation in mNO after transplantation
GFP Ki67 Nuclei
% of Ki67+ tumor cells
Day post co-culture
d10
d20
d30
d40
d
mHGG #1 stemness in mNO after transplantation
GFP Sox2 Nuclei
% of Sox2+ tumor cells
Day post co-culture

Figure 10. Engraftment and proliferation of mHGG cells following transplantation into mNO. (**a**) Schematic workflow for mHGG cell transplantation into 30-day-old mouse neural organoids (mNO), followed by dynamic culture and immunofluorescence analysis at 10-, 20-, 30-, and 40-days post-transplantation. (**b**) Representative immunofluorescence images showing widespread distribution of GFP+ mHGG cells (green) in mNO over time. Nuclei are counterstained in blue. Scale bars: 500 μm. (**c**) Representative immunofluorescence images showing GFP+ tumor cells (green) and Ki67+ proliferating cells (red). Close ups show proliferating tumor cells. Nuclei are stained in blue. On the right, boxplot represents the quantification of the percentage of GFP+ tumor cells co-expressing Ki67. Each point represents a section of an organoid analyzed. (**d**) Representative immunofluorescence images showing GFP+ tumor cells (green) and Sox2+ cells (red). Nuclei are stained in blue. On the right, boxplot represents the quantification of the percentage of GFP+ tumor cells co-expressing Ki67. Each point represents a section of an organoid analyzed.

4.2.3 Electroporation of mNO

At the same time, we wanted to test the hypothesis that the environment of mNO may be suitable to sustain glioma progression only at advanced stages, but not during the initial phase of tumor development. To explore whether mNO could support the earliest events of glioma progression, we decided to model tumor initiation from the very beginning, by introducing defined genetic modifications capable of inducing malignant transformation of healthy cells.

decided to first try to reproduce in vitro our in vivo model, overexpressing PDGF-B in mNO. While lentiviral or retroviral infection is commonly used for gene delivery, including in our in vivo model, their use raises biosafety concerns that limit their application in a human model. Therefore, we opted for a non-viral alternative based on the PiggyBac transposon system, which enables efficient and stable genomic integration while avoiding the risks associated with viral gene transfer.

4.2.3.1 Characterization of electroporated cells

Each organoid was electroporated with two plasmids: one encoding the transposase and the other carrying either PDGFB-EGFP or EGFP alone as negative control [Figure 11a]. In both conditions GFP fluorescent signal was visible the day after the electroporation, indicating successful delivery of the plasmid inside the cells. Quantifying electroporation efficiency in a 3D structure such as organoids is challenging, as electroporated cells are unevenly distributed and located at different depths within the tissue. However, even a limited number of successfully electroporated cells is sufficient for this experimental setting: even if a single cell undergoes oncogenic transformation, its expansion can ultimately give rise to a tumor mass. However, only organoids electroporated with PDGF-B developed tumor-like masses, composed of cells with a proliferative advantage over surrounding non-electroporated cells [Figure 11b]. This probably suggested the malignant transformation of the electroporated cells induced by PDGF-B overexpression. To further characterize the electroporated cells, organoid sections were analyzed by immunofluorescence staining. Electroporated cells expressed progenitor/stem cells markers such as Nestin and Sox2, as well as Ki67. They also expressed oligodendrocytes lineage-specific markers, such as Olig2 and NG2 [Figure 11c]. Contrarily, they did not express neuronal and astroglia markers, being negative for NeuN and GFAP. NeuN expression was still detectable in neighboring GFP negative cells within the organoid, indicating that non-electroporated cells retained their capacity for neuronal differentiation [data not shown]. These features matched the markers expressed by gliomas generated in vivo by PDGF-B overexpression, suggesting the possible malignant transformation of cell within mNO.

To assess whether the electroporated cells resembled more LGG or HGG cells, organoids with visible tumor-like masses at 30 days post-electroporation were dissociated into single cells and either: (1) plated in culture to test their ability to expand, or (2) co-cultured with naïve 30 days old mNO to evaluate their capacity to engraft in another organoid [Figure 11d, left panel]. HGG cells are known to proliferate in vitro and infiltrate organoid tissue, while LGG cells failed to do so. While cells derived from control organoids were negative for GFP and failed to attach to the culture, cells derived from PDGF-B electroporated organoids were predominantly GFP+ and were propagated in culture [Figure 11d, central panel]. Moreover, upon re-engraftment into naïve mNO, these cells, these cells successfully colonized the tissue and formed tumor-like masses resembling those generated by mHGG cells obtained via in utero electroporation [Figure 11d, right panel]. These findings demonstrate that PDGF-B overexpression in mNO induces the formation of cells capable of self-renewal, culture propagation and engraftment into a brain-like microenvironment, which are characteristics of mHGG. The ultimate validation of their tumorigenic potential will require transplantation into mice, which we plan as a next step. Collectively, these results indicated that mNO were capable of sustaining glioma progression from the earliest oncogenic event through advanced tumor-like stages, thereby recapitulating gliomagenesis.

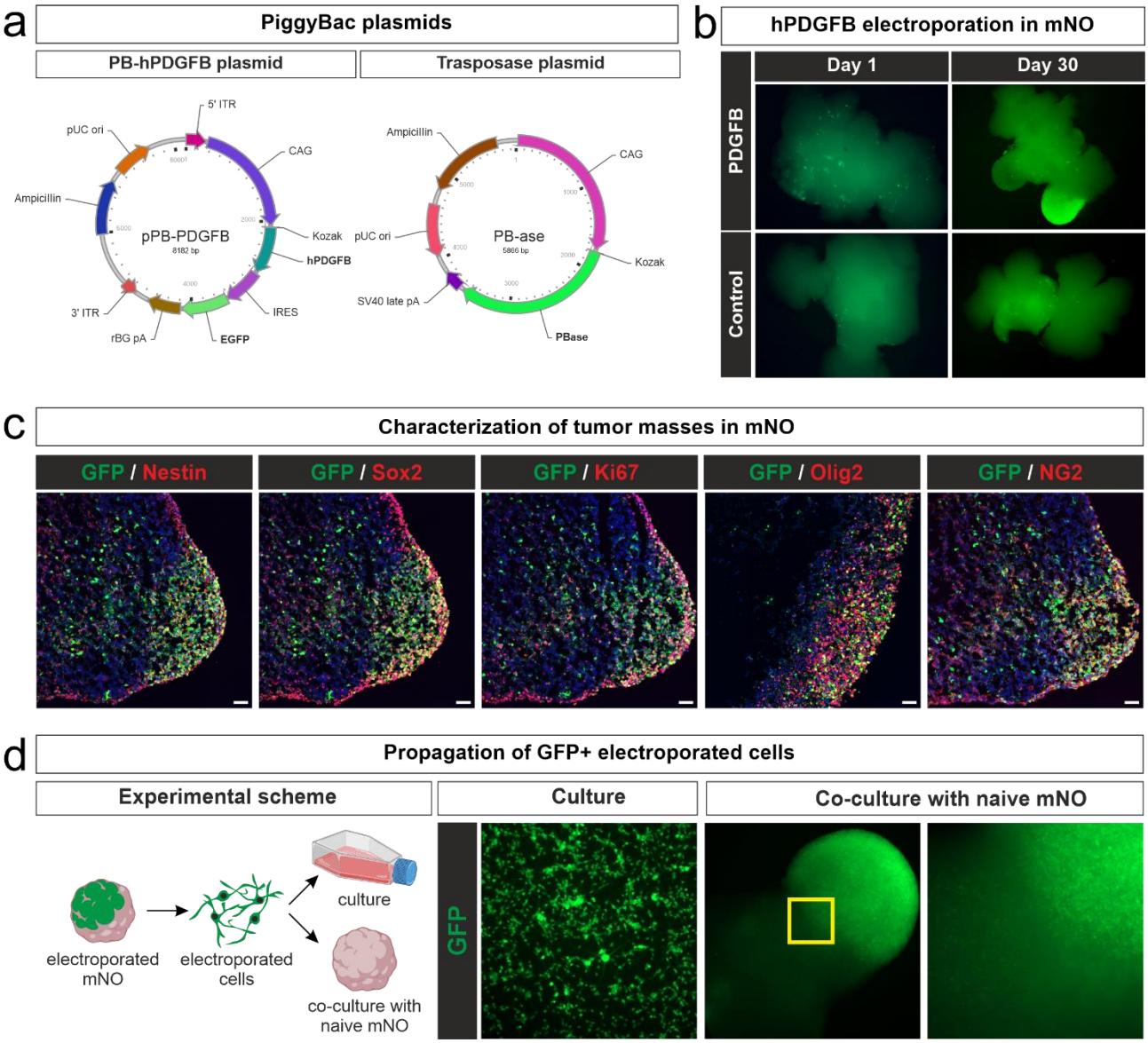

Figure 11. Electroporation of mouse neural organoids (mNO) with PDGF-B. (**a**) Schematic representation of the PiggyBac plasmids used: the PB-hPDGFB plasmid encoding PDGFB-EGFP and the PB-ase plasmid encoding the transposase. (**b**) GFP fluorescence imaging of electroporated mNO at day 1 and day 30. While both PDGFB and control organoids showed GFP signal, only PDGFB-electroporated organoids developed tumor-like masses over time. (**c**) Immunofluorescence staining of PDGFB-electroporated organoids showing GFP+ cells (green) co-expressing Nestin, Sox2, Ki67, Olig2, and NG2 (red in each panel), indicating progenitor/stem-like and oligodendrocytic lineage identity. Nuclei are stained in blue. Scale bars: 50 µm. (**d**) In the left panel, the experimental workflow: electroporated organoids were dissociated and tested for (i) expansion in culture and (ii) engraftment into nave mNO. GFP+ cells derived from PDGFB-electroporated organoids expanded in vitro (central panel) and successfully colonized naïve organoids, forming tumor-like masses (right panel).

4.3 Moving from mouse to human model

We initially developed a murine neural organoid model to complement our in vivo experiments in murine animal models. This system allowed us to optimize key experimental parameters in a setting consistent with the biology of murine gliomas. However, due to the inherent species-specific differences and the need for higher translational relevance, we plan to transition to human neural organoids. With the murine model validated, the human system provides a more representative environment to investigate glioma behavior and tumor–microenvironment interactions in a context closer to human physiology.

A first step in this direction was taken during a research stay in Germany, where I joined the laboratory of Prof. Dr. Jovica Ninkovic at LMU Munich. During this period, I acquired expertise in culturing human induced pluripotent stem cells (iPSCs), differentiating them into human neural organoids (hNO), and performing tumor cell transplantation into hNO.

4.3.1 Transplantation of mHGG cells into human neural organoids

Human neural organoids (hNO) were developed from human induced pluripotent stem cells (iPSC) ISFi001-A, seeded at a density of 9000 cells/well of a ULA 96-well plate to form embryoid bodies. On day 5, the embryoid bodies were directed toward either dorsal or ventral neural induction. On day 13, a dorsal and a ventral organoid were embedded together in a Matrigel droplet, allowing them to fuse and generate a neural assembloid. On day 17, the fused organoids were transferred to an orbital shaker and maintained under agitation until day 105-110, when they were transplanted with 2000 mHGG cells per organoid. The transplanted organoids were kept in culture for 30 days, then fixed for immunofluorescence analysis [Figure 12a].

The tumor take rate was 90% (27/30 hNO analyzed). Within 30 days, the transplanted organoids developed multifocal tumor masses of various sizes detected by fluorescent microscopy, recapitulating tumor cell behavior in vivo [Figure 12b]. mHGG cells in hNO tended to form bulbs with different morphologies: (1) bulbs with a tumor core and a peritumoral area; (2) bulbs with a tumor core but no peritumoral area; (3) bulbs with no core and only sparse cells [Figure 12c]. The tumor core is defined as an area composed solely of tumor cells, while the peritumoral area contains both cancerous and non-cancerous cells. After 30 days post-transplantation, 50.9±8.1% of mHGG cells were Ki67+ and 90.3±4.8% were Sox2+, indicating that tumor cells proliferate and maintain stem-like properties [Figure 12d-e].

One of the key features of the hNO used is the development of microglia. Therefore, we investigated the interaction between mHGG cells and microglia. Interestingly, in the presence of mHGG cells, microglia exhibited an amoeboid morphology, typical of an activated state. Moreover, some microglia cells are in contact with mHGG cells, suggesting possible phagocytic activity. In contrast, in tumor-free area the microglia displayed a ramified, homeostatic morphology [Figure 12f]. This suggests that microglia in hNO can respond to the presence of mHGG cells, becoming activated by them.

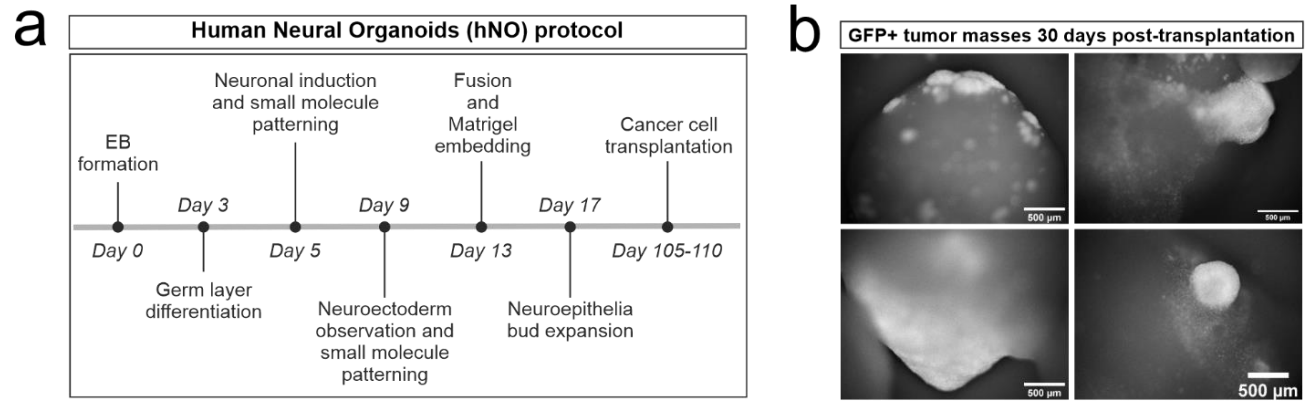
a
Human Neural Organoids (hNO) protocol
EB formation
Day 0
Day 3
Germ layer differentiation
Neuronal induction and small molecule patterning
Day 5
Day 9
Neuroectoderm observation and small molecule patterning
Fusion and Matrigel embedding
Day 13
Day 17
Neuroepithelia bud expansion
Cancer cell transplantation
Day 105-110
b
GFP+ tumor masses 30 days post-transplantation
500 µm
c
Morphology of tumor masses in hNO
GFP / Nuclei
Core + peritumoral area
Core + NO peritumoral area
NO core (sparse cells)
d
Proliferation and stemness of mHGG in hNO
GFP
Ki67
Merge
GFP
Sox2
Merge
e
% of GFP+ and Ki67+/Sox2+
100%
75%
50%
25%
0%
Ki67
sox2
channel
f
Interaction of tumor cells with microglia
GFP / GFAP / Iba1
GFP
Iba1
50 µm
Nuclei / GFP / GFAP / Iba1
20 µm

Figure 12. Transplantation of murine high-grade glioma (mHGG) cells into human neural organoids (hNO). (**a**) Overview of the protocol for the transplantation of mHGG cells into human neural organoids (hNO). iPSCs were seeded in ULA 96-well plates to form embryoid bodies. On day 5, embryoid bodies were directed toward either dorsal or ventral neural induction. On day 13, a dorsal and a ventral organoid were embedded together in a Matrigel droplet and fused, generating a neural organoid with dorsal-ventral polarity. On day 17, fused organoids were transferred to an orbital shaker and maintained in agitation until day 105, when they were transplanted with mHGG cells. Transplanted organoids were cultured for 30 days before fixation and immunofluorescence analysis. **(b)** Immunofluorescence images of transplanted hNO at 30 days post-transplantation. GFP fluorescence reveals multifocal masses of mHGG cells growing within the organoid. Scale bars = 500 µm. **(c)** Fluorescence images showing mHGG cell distribution across hNO sections. Tumor cells (GFP, green) and nuclei (Hoechst, blue) reveal three distinct growth patterns: (1) tumor core with peritumoral area, (2) core without peritumoral area, and (3) sparse cells without a defined core. **(d)** Immunofluorescence staining of transplanted hNO sections after 30 days, showing expression of Ki67 (magenta) and Sox2 (magenta) in GFP+ (green) tumor cells. Hoechst stains nuclei (blue). Scale bars = 500 µm or 100 µm. **(e)** Quantification of the percentage of GFP+ tumor cells co-expressing Ki67 or Sox2 across individual hNO sections. Error bars represent standard error of the mean. **(f)** Maximum intensity projection of confocal z-stacks showing interaction between mHGG cells (GFP, green), astrocytes (GFAP, magenta), microglia (Iba1, yellow), and nuclei (Hoechst, blue). Insets show a tumor region with amoeboid, activated microglia (yellow box) and a tumor-free region with ramified, homeostatic microglia (light blue box). Scale bars = 500 µm, 50 µm (magnifications). Right panel: orthogonal projection highlights direct contact between an activated microglia cell and a mHGG cell. Scale bar = 20 µm.

5 Discussion

Glioblastoma (GBM) is a highly aggressive and heterogeneous brain tumor, characterized by diffuse infiltration, high cellular plasticity, and resistance to conventional therapies. Despite decades of research, prognosis remains dismal, with median survival rarely exceeding 15 months[4]. One of the major obstacles in GBM research is the lack of experimental models that faithfully recapitulate the complexity of the disease. Many preclinical models have failed to predict therapeutic efficacy in patients, limiting the translational impact of preclinical discoveries[29,79].

In vitro 2D models (tumor cell lines and spheroids) are cost-effective and easy to manipulate, but lack the three-dimensional architecture, cellular heterogeneity, and tumor–microenvironment (TME) interactions of GBM[35,36]. In vivo models (syngeneic and xenograft mouse models, or genetically engineered mouse models) offer a more physiological context, enabling the study of angiogenesis, immune responses, and therapeutic effects in a living [43]. However, they are limited by species-specific differences between rodents and humans and ethical concerns associated with the use of animals[43]. More recently, organoid-based models have emerged as a promising alternative, bridging in vitro and in vivo approaches: they preserve tissue-like cytoarchitecture and multiple cellular lineages, while remaining accessible to genetic manipulation and therapeutic testing[63,89,104,113].

The aim of this thesis was to establish neural organoid-based models to study gliomagenesis and glioma progression, complementing our in vivo model based on Platelet-Derived Growth Factor B (PDGF-B) overexpression in mouse embryos. Given the absence of prior expertise in our group, we first optimized the generation of mouse neural organoids (mNO), adapting the Lancaster and Knoblich protocol[70] to murine cells. As for human organoid protocols, we initiated the differentiation from mouse embryonic stem cells (mESCs). These cells were maintained under feeder-free conditions on Matrigel-coated plates in the presence of inhibitors targeting the FGF/ERK signaling pathway, in order to preserve a pluripotent state that demonstrated to be compatible with subsequent neural differentiation. Under these conditions, mESCs exhibited robust expression of pluripotency markers, including Sox2 and Oct3/4, confirming the maintenance of an undifferentiated state suitable for organoid generation. During the 30 days of differentiation, mNO exhibited features of correctly differentiated organoids, such as neural rosettes reminiscent of the neural tube, alongside differentiated neurons and astrocytes, both relevant for tumor-host interactions. Positional markers such as Foxg1 or Nkx2.1 were not addressed since the aim of this thesis was not to model a specific brain area, but to establish a 3D neural microenvironment capable of supporting tumor growth, invasion and tumor-host interactions. For this purpose, the presence of organized neural tissue containing progenitors, neurons, and astrocytes was more relevant than strict regional specification. Future work could nonetheless include positional marker analysis to further refine the characterization of the model. A certain degree of immaturity is an intrinsic feature of neural organoids, which more closely recapitulate neurodevelopment rather than adult brain stages. Indeed, current neural organoid models are unable to fully reproduce the complexity and maturation state of the adult brain[70,71,134] and the generation, and maintenance of long-

term, highly mature organoids remain technically challenging. For these reasons, we selected this differentiation timepoint for subsequent experiments, as it represents the earliest stage at which all cell types of interest were detected. Moreover, for specific experimental approaches (such as the electroporation of mNO) using organoids that more closely resemble the embryonic brain environment allowed better alignment with our in vivo model. This choice also reflected the need for a practical and time-efficient experimental framework, given the long time scales required for downstream tumor growth and progression studies. Conversely, we demonstrated that the differentiation protocol was not suitable for the differentiation of organoids starting from neural progenitor cells, probably due to their already committed differentiation.

Once obtained mNO with the suitable cell types, we tried two main approaches to generate gliomas: (1) a cell-based approach, that involved the inoculation of primary murine glioma cells (either high-grade or low-grade) in mNO through co-culture or direct transplantation, allowing tumor cells to grow within the organoid environment; (2) a genetic-based approach, that relied on the genetic modification of healthy cells in mNO to induce malignant transformation and tumor formation.

The first approach was designed to address a key limitation of our in vivo model: mouse low-grade glioma (mLGG) cells cannot be maintained in culture, which forced us to generate them de novo by embryonic injections each time they were needed and prevented us to fully characterize them. To optimize the method, we used mouse high-grade glioma cells (mHGG), that, contrarily to the LGGs, can be propagated in vitro over extended periods. Our data confirmed that mNO provided a supportive microenvironment for mHGG, with engraftment rates superior to 95% and preservation of both proliferative and stem-like features over time. Interestingly, the two HGG lines tested displayed different behaviors: mHGG#1 formed mainly localized tumor masses, while mHGG#2 exhibited rapid and aggressive proliferation into the organoid parenchyma, reflecting clinically relevant heterogeneity. Dynamic monitoring with Gaussia luciferase confirmed early engraftment and tumor growth. Although a small proportion of apoptotic cells emerged at later stages, the majority of tumor cells remained proliferative, confirming the capacity of mNO to sustain glioma expansion. However, when the method was applied to LGGs, the co-culture approach failed: tumor cells did not engraft in mNO. Similarly, co-culture with human neural organoids (hNO), including those with hyper-excitable characteristics, did not result in detectable integration of mLGG. We speculated that co-culture may not be suitable for mLGG, which lack fully developed invasive properties. We therefore explored direct transplantation of tumor cells into the organoid parenchyma. Using mHGG as a proof-of-concept, we demonstrated stable engraftment, expansion and maintenance of proliferative and stem-like features for more than one month post-transplantation. This method will next be tested with mLGG, to determine whether direct delivery in the organoid parenchyma provides a more reliable strategy to establish tumor-bearing organoids and to study glioma growth dynamics in a controlled microenvironment.

At the same time, we wondered whether mNO could serve as a suitable platform to model glioma progression from such early stages. To address this, we aimed to reproduce gliomagenesis de novo within organoids, using a genetic approach aimed to generate an in vitro

model capable of capturing the early events of gliomagenesis, immediately following the genetic alteration. To this end, we applied established strategies for organoid[122–124], and overexpressed PDGF-B using the PiggyBac transposon system in mNO. This induced the formation of tumor-like masses composed of proliferative, stem-like cells. These cells expressed markers consistent with the gliomas generated in vivo and could be propagated both in culture and upon re-engraftment into naïve organoids. In contrast, cells isolated from control organoids (mNO electroporated with the fluorescent reporter only) were negative for reporter expression and failed to attach to the culture dish. The absence of reporter-positive cells is not unexpected, given the low number of electroporated cells detectable 30 days after electroporation. The inability of these cells to attach in culture is more surprising, as Sox2+ progenitors are generally capable of adherence and expansion; however, in this context they likely represent only a minor fraction of the total organoid cell population, which may account for their limited survival and growth under standard culture conditions. Unlike controls, cells overexpressing PDGFb exhibited features more closely resembling high-grade gliomas, suggesting that this method can generate de novo tumor cells directly within organoids and thus provide a valuable platform to model gliomagenesis in a controlled environment. Future work will involve transcriptomic profiling to determine whether their expression signatures align more with mLGG, mHGG or an intermediate state, as well as transplantation into syngeneic mice to confirm their tumorigenic potential.

Transitioning from murine to human neural organoids represents a crucial step toward translational relevance. While mouse organoids allowed optimization of experimental parameters and to address specific questions related to the murine glioma model in use in the group, human organoids provide a species-specific context to study glioma–microenvironment interactions. Transplantation of mHGG into hNO resulted in high engraftment rate and the formation of tumor-like masses with heterogeneous growth patterns. Tumor cells remained highly proliferative and retained stem-like properties. Importantly, the presence of microglia within hNO enabled the observation of tumor–immune interactions: microglia adopted an activated phenotype upon contact with glioma cells, highlighting a dynamic response that is absent in models lacking immune components. This provided proof-of-concept that organoid-derived immune populations can interact with tumor cells in a manner resembling in vivo conditions.

In conclusion, this thesis showed that neural organoids can sustain glioma growth, preserve stemness, and recapitulate key aspects of tumor–microenvironment interactions. By bridging the gap between traditional in vitro models and animal systems, organoid-based approaches provide unique opportunities to study GBM biology and to develop more effective therapies. While challenges remain, particularly regarding vascularization and immune integration, the advances presented here contribute to the growing recognition of organoids as essential tools in neuro-oncology.

6 Conclusion

This thesis confirmed the feasibility and utility of organoid-based systems for modeling glioma progression. Mouse neural organoids allowed us to establish and optimize an in vitro model of glioma progression that supported the engraftment and proliferation of high-grade gliomas, while highlighting some difficulties with less invasive low-grade gliomas that probably need more direct delivery of cells into the organoid parenchyma. The genetic engineering of organoids via PDGF-B overexpression provided a proof-of-principle that gliomagenesis can be induced de novo within a mouse organoid system, opening the way to study the earliest steps of tumor initiation. Transitioning to human neural organoids represented an important step towards translational relevance. Initial experiments on human neural organoids revealed that high-grade glioma cells engrafted efficiently, retaining proliferative and stem-like features, and induced microglia activation, recapitulating an important aspect of the human tumor microenvironment. Collectively, these findings establish neural organoids as an intermediate platform bridging the gap between traditional in vitro systems and animal models, enabling the study of glioma dynamics and progression in an in vitro context, both murine and human.

7 References

1. Van Den Bent, M. J. *et al.* Primary brain tumours in adults. *The Lancet* **402**, 1564–1579 (2023).
2. Louis, D. N. *et al.* The 2021 WHO Classification of Tumors of the Central Nervous System: a summary. *Neuro-Oncol.* **23**, 1231–1251 (2021).
3. Whitfield, B. T. & Huse, J. T. Classification of adult-type diffuse gliomas: Impact of the World Health Organization 2021 update. *Brain Pathol.* **32**, e13062 (2022).
4. Ostrom, Q. T. *et al.* CBTRUS Statistical Report: Primary Brain and Other Central Nervous System Tumors Diagnosed in the United States in 2016—2020. *Neuro-Oncol.* **25**, iv1–iv99 (2023).
5. Stupp, R. *et al.* Radiotherapy plus concomitant and adjuvant temozolomide for glioblastoma. *N. Engl. J. Med.* **352**, 987–996 (2005).
6. Schaff, L. R. & Mellinghoff, I. K. Glioblastoma and other Primary Brain Malignancies in Adults. A Review. *JAMA* **329**, 574–587 (2023).
7. Stupp, R. *et al.* Effect of Tumor-Treating Fields Plus Maintenance Temozolomide vs Maintenance Temozolomide Alone on Survival in Patients With Glioblastoma: A Randomized Clinical Trial. *JAMA* **318**, 2306–2316 (2017).
8. Hegi, M. E. *et al.* MGMT gene silencing and benefit from temozolomide in glioblastoma. *N. Engl. J. Med.* **352**, 997–1003 (2005).
9. Wen, P. Y. *et al.* Glioblastoma in adults: a Society for Neuro-Oncology (SNO) and European Society of Neuro-Oncology (EANO) consensus review on current management and future directions. *Neuro-Oncol.* **22**, 1073–1113 (2020).
10. Jung, E. *et al.* Emerging intersections between neuroscience and glioma biology. *Nat. Neurosci.* **22**, 1951–1960 (2019).
11. Daou, M.-C., Smith, T. W., Litofsky, N. S., Hsieh, C. C. & Ross, A. H. Doublecortin is preferentially expressed in invasive human brain tumors. *Acta Neuropathol. (Berl.)* **110**, 472–480 (2005).
12. Osswald, M. *et al.* Brain tumour cells interconnect to a functional and resistant network. *Nature* **528**, 93–98 (2015).
13. Tsai, J.-W., Bremner, K. H. & Vallee, R. B. Dual subcellular roles for LIS1 and dynein in radial neuronal migration in live brain tissue. *Nat. Neurosci.* **10**, 970–979 (2007).
14. Osswald, M., Solecki, G., Wick, W. & Winkler, F. A malignant cellular network in gliomas: potential clinical implications. *Neuro-Oncol.* **18**, 479–485 (2016).
15. Venkataramani, V. *et al.* Glioblastoma hijacks neuronal mechanisms for brain invasion. *Cell* **185**, 2899-2917.e31 (2022).
16. Venkataramani, V. *et al.* Glutamatergic synaptic input to glioma cells drives brain tumour progression. *Nature* **573**, 532–538 (2019).
17. Buckingham, S. C. *et al.* Glutamate release by primary brain tumors induces epileptic activity. *Nat. Med.* **17**, 1269–1274 (2011).
18. Tobochnik, S. *et al.* Pilot Trial of Perampanel on Peritumoral Hyperexcitability in Newly Diagnosed High-grade Glioma. *Clin. Cancer Res. Off. J. Am. Assoc. Cancer Res.* **30**, 5365–5373 (2024).

19. Venkatesh, H. S. *et al.* Electrical and synaptic integration of glioma into neural circuits. *Nature* **573**, 539–545 (2019).
20. Yabo, Y. A., Niclou, S. P. & Golebiewska, A. Cancer cell heterogeneity and plasticity: A paradigm shift in glioblastoma. *Neuro-Oncol.* **24**, 669–682 (2022).
21. Uribe, D. *et al.* Adapt to Persist: Glioblastoma Microenvironment and Epigenetic Regulation on Cell Plasticity. *Biology* **11**, 313 (2022).
22. Verhaak, R. G. W. *et al.* Integrated genomic analysis identifies clinically relevant subtypes of glioblastoma characterized by abnormalities in PDGFRA, IDH1, EGFR, and NF1. *Cancer Cell* **17**, 98–110 (2010).
23. Bhat, K. P. L. *et al.* Mesenchymal Differentiation Mediated by NF-κB Promotes Radiation Resistance in Glioblastoma. *Cancer Cell* **24**, 331–346 (2013).
24. Lau, J. *et al.* STAT3 Blockade Inhibits Radiation-Induced Malignant Progression in Glioma. *Cancer Res.* **75**, 4302–4311 (2015).
25. Halliday, J. *et al.* In vivo radiation response of proneural glioma characterized by protective p53 transcriptional program and proneural-mesenchymal shift. *Proc. Natl. Acad. Sci.* **111**, 5248–5253 (2014).
26. Sottoriva, A. *et al.* Intratumor heterogeneity in human glioblastoma reflects cancer evolutionary dynamics. *Proc. Natl. Acad. Sci.* **110**, 4009–4014 (2013).
27. Neftel, C. *et al.* An Integrative Model of Cellular States, Plasticity, and Genetics for Glioblastoma. *Cell* **178**, 835-849.e21 (2019).
28. Aldape, K. *et al.* Challenges to curing primary brain tumours. *Nat. Rev. Clin. Oncol.* **16**, 509–520 (2019).
29. Lenting, K., Verhaak, R., ter Laan, M., Wesseling, P. & Leenders, W. Glioma: experimental models and reality. *Acta Neuropathol. (Berl.)* **133**, 263–282 (2017).
30. Benda, P., Lightbody, J., Sato, G., Levine, L. & Sweet, W. Differentiated rat glial cell strain in tissue culture. *Science* **161**, 370–371 (1968).
31. Ausman, J. I., Shapiro, W. R. & Rall, D. P. Studies on the chemotherapy of experimental brain tumors: development of an experimental model. *Cancer Res.* **30**, 2394–2400 (1970).
32. Genoud, V. *et al.* Responsiveness to anti-PD-1 and anti-CTLA-4 immune checkpoint blockade in SB28 and GL261 mouse glioma models. *Oncoimmunology* **7**, e1501137 (2018).
33. Pontén, J. & Macintyre, E. H. Long Term Culture of Normal and Neoplastic Human Glia. *Acta Pathol. Microbiol. Scand.* **74**, 465–486 (1968).
34. Pasupuleti, V., Vora, L., Prasad, R., Nandakumar, D. N. & Khatri, D. K. Glioblastoma preclinical models: Strengths and weaknesses. *Biochim. Biophys. Acta Rev. Cancer* **1879**, 189059 (2024).
35. Xie, Y. *et al.* The Human Glioblastoma Cell Culture Resource: Validated Cell Models Representing All Molecular Subtypes. *EBioMedicine* **2**, 1351–1363 (2015).
36. Idrisova, K. F., Simon, H.-U. & Gomzikova, M. O. Role of Patient-Derived Models of Cancer in Translational Oncology. *Cancers* **15**, 139 (2022).
37. Weiswald, L.-B., Bellet, D. & Dangles-Marie, V. Spherical cancer models in tumor biology. *Neoplasia N. Y. N* **17**, 1–15 (2015).
38. Singh, S. K. *et al.* Identification of a cancer stem cell in human brain tumors. *Cancer Res.* **63**, 5821–5828 (2003).

39. Thomas, G. & Rahman, R. Evolution of Preclinical Models for Glioblastoma Modelling and Drug Screening. *Curr. Oncol. Rep.* **27**, 601–624 (2025).
40. Griffin, C. P. *et al.* Postmortem brain donations vs premortem surgical resections for glioblastoma research: viewing the matter as a whole. *Neuro-Oncol. Adv.* **4**, vdab168 (2022).
41. Ravi, V. M. *et al.* Human organotypic brain slice culture: a novel framework for environmental research in neuro-oncology. *Life Sci. Alliance* **2**, e201900305 (2019).
42. Greene, H. S. N. & Arnold, H. The Homologous and Heterologous Transplantation of Brain and Brain Tumors. https://doi.org/10.3171/jns.1945.2.4.0315 (1945) doi:10.3171/jns.1945.2.4.0315.
43. Sahu, U., Barth, R. F., Otani, Y., McCormack, R. & Kaur, B. Rat and Mouse Brain Tumor Models for Experimental Neuro-Oncology Research. *J. Neuropathol. Exp. Neurol.* **81**, 312–329 (2022).
44. Chinwalla, A. T. *et al.* Initial sequencing and comparative analysis of the mouse genome. *Nature* **420**, 520–562 (2002).
45. Slika, H. *et al.* Preclinical Models and Technologies in Glioblastoma Research: Evolution, Current State, and Future Avenues. *Int. J. Mol. Sci.* **24**, 16316 (2023).
46. Liu, P. *et al.* Preclinical models of glioblastoma: limitations of current models and the promise of new developments. *Expert Rev. Mol. Med.* **23**, e20 (2021).
47. Joo, K. M. *et al.* Patient-specific orthotopic glioblastoma xenograft models recapitulate the histopathology and biology of human glioblastomas in situ. *Cell Rep.* **3**, 260–273 (2013).
48. Use of Retroviral and Lentiviral Vectors to Deliver New Gene Therapies - MedCrave online. https://medcraveonline.com/JHVRV/use-of-retroviral-and-lentiviral-vectors-to-deliver-new-gene-therapies.html.
49. Calzolari, F. *et al.* Tumor progression and oncogene addiction in a PDGF-B-induced model of gliomagenesis. *Neoplasia N. Y. N* **10**, 1373–1382, following 1382 (2008).
50. Pradhan, R. K. & Ramakrishna, W. Transposons: Unexpected players in cancer. *Gene* **808**, 145975 (2022).
51. Ivics, Z., Hackett, P. B., Plasterk, R. H. & Izsvák, Z. Molecular reconstruction of Sleeping Beauty, a Tc1-like transposon from fish, and its transposition in human cells. *Cell* **91**, 501–510 (1997).
52. Sumiyoshi, K., Koso, H. & Watanabe, S. Spontaneous development of intratumoral heterogeneity in a transposon-induced mouse model of glioma. *Cancer Sci.* **109**, 1513–1523 (2018).
53. Núñez, F. J. *et al.* IDH1-R132H acts as a tumor suppressor in glioma via epigenetic up-regulation of the DNA damage response. *Sci. Transl. Med.* **11**, eaaq1427 (2019).
54. Zhao, S. *et al.* PiggyBac transposon vectors: the tools of the human gene encoding. *Transl. Lung Cancer Res.* **5**, 120–125 (2016).
55. Chen, F., Becker, A. & LoTurco, J. Overview of Transgenic Glioblastoma and Oligoastrocytoma CNS Models and Their Utility in Drug Discovery. *Curr. Protoc. Pharmacol.* **72**, 14.37.1-14.37.12 (2016).
56. McLellan, M. A., Rosenthal, N. A. & Pinto, A. R. Cre-loxP-Mediated Recombination: General Principles and Experimental Considerations. *Curr. Protoc. Mouse Biol.* **7**, 1–12 (2017).

57. Jun, H. J. *et al.* A PDGFRα-driven mouse model of glioblastoma reveals a stathmin1-mediated mechanism of sensitivity to vinblastine. *Nat. Commun.* **9**, 3116 (2018).
58. Alcantara Llaguno, S. *et al.* Cell-of-origin susceptibility to glioblastoma formation declines with neural lineage restriction. *Nat. Neurosci.* **22**, 545–555 (2019).
59. Jinek, M. *et al.* A programmable dual-RNA-guided DNA endonuclease in adaptive bacterial immunity. *Science* **337**, 816–821 (2012).
60. Boddu, P. C. *et al.* Generation of scalable cancer models by combining AAV-intron-trap, CRISPR/Cas9, and inducible Cre-recombinase. *Commun. Biol.* **4**, 1184 (2021).
61. Zhan, T., Rindtorff, N., Betge, J., Ebert, M. P. & Boutros, M. CRISPR/Cas9 for cancer research and therapy. *Semin. Cancer Biol.* **55**, 106–119 (2019).
62. Oldrini, B. *et al.* Somatic genome editing with the RCAS-TVA-CRISPR-Cas9 system for precision tumor modeling. *Nat. Commun.* **9**, 1466 (2018).
63. Chiaradia, I. & Lancaster, M. A. Brain organoids for the study of human neurobiology at the interface of in vitro and in vivo. *Nat. Neurosci.* **23**, 1496–1508 (2020).
64. Pașca, S. P. *et al.* A nomenclature consensus for nervous system organoids and assembloids. *Nature* **609**, 907–910 (2022).
65. Li, W. *et al.* Rapid induction and long-term self-renewal of primitive neural precursors from human embryonic stem cells by small molecule inhibitors. *Proc. Natl. Acad. Sci. U. S. A.* **108**, 8299–8304 (2011).
66. Watanabe, K. *et al.* Directed differentiation of telencephalic precursors from embryonic stem cells. *Nat. Neurosci.* **8**, 288–296 (2005).
67. Watanabe, K. *et al.* A ROCK inhibitor permits survival of dissociated human embryonic stem cells. *Nat. Biotechnol.* **25**, 681–686 (2007).
68. Eiraku, M. *et al.* Self-organized formation of polarized cortical tissues from ESCs and its active manipulation by extrinsic signals. *Cell Stem Cell* **3**, 519–532 (2008).
69. Lancaster, M. A. *et al.* Cerebral organoids model human brain development and microcephaly. *Nature* **501**, 373–379 (2013).
70. Lancaster, M. A. & Knoblich, J. A. Generation of cerebral organoids from human pluripotent stem cells. *Nat. Protoc.* **9**, 2329–2340 (2014).
71. Quadrato, G. *et al.* Cell diversity and network dynamics in photosensitive human brain organoids. *Nature* **545**, 48–53 (2017).
72. Lancaster, M. A. *et al.* Guided self-organization and cortical plate formation in human brain organoids. *Nat. Biotechnol.* **35**, 659–666 (2017).
73. Giandomenico, S. L., Sutcliffe, M. & Lancaster, M. A. Generation and long-term culture of advanced cerebral organoids for studying later stages of neural development. *Nat. Protoc.* **16**, 579–602 (2021).
74. Giandomenico, S. L. *et al.* Cerebral organoids at the air-liquid interface generate diverse nerve tracts with functional output. *Nat. Neurosci.* **22**, 669–679 (2019).
75. Madhavan, M. *et al.* Induction of myelinating oligodendrocytes in human cortical spheroids. *Nat. Methods* **15**, 700–706 (2018).
76. Marton, R. M. *et al.* Differentiation and maturation of oligodendrocytes in human three-dimensional neural cultures. *Nat. Neurosci.* **22**, 484–491 (2019).

77. Ormel, P. R. *et al.* Microglia innately develop within cerebral organoids. *Nat. Commun.* **9**, 4167 (2018).
78. Paşca, A. M. *et al.* Functional cortical neurons and astrocytes from human pluripotent stem cells in 3D culture. *Nat. Methods* **12**, 671–678 (2015).
79. Birey, F. *et al.* Assembly of functionally integrated human forebrain spheroids. *Nature* **545**, 54–59 (2017).
80. Sakaguchi, H. *et al.* Generation of functional hippocampal neurons from self-organizing human embryonic stem cell-derived dorsomedial telencephalic tissue. *Nat. Commun.* **6**, 8896 (2015).
81. Xiang, Y. *et al.* hESC-Derived Thalamic Organoids Form Reciprocal Projections When Fused with Cortical Organoids. *Cell Stem Cell* **24**, 487-497.e7 (2019).
82. Qian, X. *et al.* Brain-Region-Specific Organoids Using Mini-bioreactors for Modeling ZIKV Exposure. *Cell* **165**, 1238–1254 (2016).
83. Jo, J. *et al.* Midbrain-like Organoids from Human Pluripotent Stem Cells Contain Functional Dopaminergic and Neuromelanin-Producing Neurons. *Cell Stem Cell* **19**, 248–257 (2016).
84. Muguruma, K., Nishiyama, A., Kawakami, H., Hashimoto, K. & Sasai, Y. Self-organization of polarized cerebellar tissue in 3D culture of human pluripotent stem cells. *Cell Rep.* **10**, 537–550 (2015).
85. Miura, Y. *et al.* Generation of human striatal organoids and cortico-striatal assembloids from human pluripotent stem cells. *Nat. Biotechnol.* **38**, 1421–1430 (2020).
86. Andersen, J. *et al.* Generation of Functional Human 3D Cortico-Motor Assembloids. *Cell* **183**, 1913-1929.e26 (2020).
87. Benito-Kwiecinski, S. & Lancaster, M. A. Brain Organoids: Human Neurodevelopment in a Dish. *Cold Spring Harb. Perspect. Biol.* **12**, a035709 (2020).
88. Sidhaye, J. & Knoblich, J. A. Brain organoids: an ensemble of bioassays to investigate human neurodevelopment and disease. *Cell Death Differ.* **28**, 52–67 (2021).
89. Qian, X., Song, H. & Ming, G.-L. Brain organoids: advances, applications and challenges. *Dev. Camb. Engl.* **146**, dev166074 (2019).
90. Kelley, K. W. & Paşca, S. P. Human brain organogenesis: Toward a cellular understanding of development and disease. *Cell* **185**, 42–61 (2022).
91. Gabriel, E. *et al.* CPAP promotes timely cilium disassembly to maintain neural progenitor pool. *EMBO J.* **35**, 803–819 (2016).
92. Garcez, P. P. *et al.* Zika virus impairs growth in human neurospheres and brain organoids. *Science* **352**, 816–818 (2016).
93. Cugola, F. R. *et al.* The Brazilian Zika virus strain causes birth defects in experimental models. *Nature* **534**, 267–271 (2016).
94. Retallack, H. *et al.* Zika virus cell tropism in the developing human brain and inhibition by azithromycin. *Proc. Natl. Acad. Sci. U. S. A.* **113**, 14408–14413 (2016).
95. Amin, N. D. & Paşca, S. P. Building Models of Brain Disorders with Three-Dimensional Organoids. *Neuron* **100**, 389–405 (2018).
96. Pollen, A. A. *et al.* Molecular Identity of Human Outer Radial Glia during Cortical Development. *Cell* **163**, 55–67 (2015).

97. Lewitus: Conical expansion of the outer subventricular... - Google Scholar. https://scholar.google.com/scholar_lookup?title=Conical%20expansion%20of%20the%20outer%20subventricular%20zone%20and%20the%20role%20of%20neocortical%20folding%20in%20evolution%20and%20development&author=E.%20Lewitus&publication_year=2013.
98. Bershteyn, M. *et al.* Human iPSC-Derived Cerebral Organoids Model Cellular Features of Lissencephaly and Reveal Prolonged Mitosis of Outer Radial Glia. *Cell Stem Cell* **20**, 435-449.e4 (2017).
99. Li, Y. *et al.* Induction of Expansion and Folding in Human Cerebral Organoids. *Cell Stem Cell* **20**, 385-396.e3 (2017).
100. Geschwind, D. H. Genetics of autism spectrum disorders. *Trends Cogn. Sci.* **15**, 409–416 (2011).
101. Villa, C., Combi, R., Conconi, D. & Lavitrano, M. Patient-Derived Induced Pluripotent Stem Cells (iPSCs) and Cerebral Organoids for Drug Screening and Development in Autism Spectrum Disorder: Opportunities and Challenges. *Pharmaceutics* **13**, 280 (2021).
102. Mariani, J. *et al.* FOXG1-Dependent Dysregulation of GABA/Glutamate Neuron Differentiation in Autism Spectrum Disorders. *Cell* **162**, 375–390 (2015).
103. Urresti, J. *et al.* Cortical organoids model early brain development disrupted by 16p11.2 copy number variants in autism. *Mol. Psychiatry* **26**, 7560–7580 (2021).
104. Acharya, P., Choi, N. Y., Shrestha, S., Jeong, S. & Lee, M.-Y. Brain organoids: A revolutionary tool for modeling neurological disorders and development of therapeutics. *Biotechnol. Bioeng.* **121**, 489–506 (2024).
105. Braak, H. & Braak, E. Neuropathological stageing of Alzheimer-related changes. *Acta Neuropathol. (Berl.)* **82**, 239–259 (1991).
106. Choi, S. H. *et al.* A three-dimensional human neural cell culture model of Alzheimer's disease. *Nature* **515**, 274–278 (2014).
107. Kim, Y. H. *et al.* A 3D human neural cell culture system for modeling Alzheimer's disease. *Nat. Protoc.* **10**, 985–1006 (2015).
108. Fearnley, J. M. & Lees, A. J. AGEING AND PARKINSON'S DISEASE: SUBSTANTIA NIGRA REGIONAL SELECTIVITY. *Brain* **114**, 2283–2301 (1991).
109. Spillantini, M. G. *et al.* α-Synuclein in Lewy bodies. *Nature* **388**, 839–840 (1997).
110. Di Fonzo, A. *et al.* A frequent *LRRK2* gene mutation associated with autosomal dominant Parkinson's disease. *The Lancet* **365**, 412–415 (2005).
111. Chesselet, M.-F., Fleming, S., Mortazavi, F. & Meurers, B. Strengths and limitations of genetic mouse models of Parkinson's disease. *Parkinsonism Relat. Disord.* **14 Suppl 2**, S84-87 (2008).
112. Kim, H. *et al.* Modeling G2019S-LRRK2 Sporadic Parkinson's Disease in 3D Midbrain Organoids. *Stem Cell Rep.* **12**, 518–531 (2019).
113. Next-Generation Regenerative Medicine: Organogenesis from Stem Cells in 3D Culture: Cell Stem Cell. https://www.cell.com/cell-stem-cell/fulltext/S1934-5909(13)00145-8?_returnURL=https%3A%2F%2Flinkinghub.elsevier.com%2Fretrieve%2Fpii%2FS1934590913001458%3Fshowall%3Dtrue.

114. Hubert, C. G. *et al.* A Three-Dimensional Organoid Culture System Derived from Human Glioblastomas Recapitulates the Hypoxic Gradients and Cancer Stem Cell Heterogeneity of Tumors Found In Vivo. *Cancer Res.* **76**, 2465–2477 (2016).
115. Jacob, F. *et al.* A Patient-Derived Glioblastoma Organoid Model and Biobank Recapitulates Inter- and Intra-tumoral Heterogeneity. *Cell* **180**, 188-204.e22 (2020).
116. Wen, J. *et al.* Applications of organoid technology to brain tumors. *CNS Neurosci. Ther.* **29**, 2725–2743 (2023).
117. Linkous, A. *et al.* Modeling Patient-Derived Glioblastoma with Cerebral Organoids. *Cell Rep.* **26**, 3203-3211.e5 (2019).
118. Azzarelli, R., Ori, M., Philpott, A. & Simons, B. D. Three-dimensional model of glioblastoma by co-culturing tumor stem cells with human brain organoids. *Biol. Open* **10**, bio056416 (2021).
119. da Silva, B., Mathew, R. K., Polson, E. S., Williams, J. & Wurdak, H. Spontaneous Glioblastoma Spheroid Infiltration of Early-Stage Cerebral Organoids Models Brain Tumor Invasion. *SLAS Discov. Adv. Life Sci. R D* **23**, 862–868 (2018).
120. Krieger, T. G. *et al.* Modeling glioblastoma invasion using human brain organoids and single-cell transcriptomics. *Neuro-Oncol.* **22**, 1138–1149 (2020).
121. Jermakowicz, A. M. *et al.* The novel BET inhibitor UM-002 reduces glioblastoma cell proliferation and invasion. *Sci. Rep.* **11**, 23370 (2021).
122. Lago, C. *et al.* Medulloblastoma and high-grade glioma organoids for drug screening, lineage tracing, co-culture and in vivo assay. *Nat. Protoc.* **18**, 2143–2180 (2023).
123. Bian, S. *et al.* Genetically engineered cerebral organoids model brain tumor formation. *Nat. Methods* **15**, 631–639 (2018).
124. Ogawa, J., Pao, G. M., Shokhirev, M. N. & Verma, I. M. Glioblastoma Model Using Human Cerebral Organoids. *Cell Rep.* **23**, 1220–1229 (2018).
125. Appolloni, I. *et al.* Progression from low- to high-grade in a glioblastoma model reveals the pivotal role of immunoediting. *Cancer Lett.* **442**, 213–221 (2019).
126. Ceresa, D. *et al.* Early clonal extinction in glioblastoma progression revealed by genetic barcoding. *Cancer Cell* **41**, 1466-1479.e9 (2023).
127. Tamm, C., Pijuan Galitó, S. & Annerén, C. A comparative study of protocols for mouse embryonic stem cell culturing. *PloS One* **8**, e81156 (2013).
128. Watanabe, K. *et al.* Directed differentiation of telencephalic precursors from embryonic stem cells. *Nat. Neurosci.* **8**, 288–296 (2005).
129. Eiraku, M. *et al.* Self-organized formation of polarized cortical tissues from ESCs and its active manipulation by extrinsic signals. *Cell Stem Cell* **3**, 519–532 (2008).
130. Martins-Costa, C. *et al.* Morphogenesis and development of human telencephalic organoids in the absence and presence of exogenous extracellular matrix. *EMBO J.* **42**, e113213 (2023).
131. Hu, X. *et al.* Expression of p53, epidermal growth factor receptor, Ki-67 and O6-methylguanine-DNA methyltransferase in human gliomas. *Oncol. Lett.* **6**, 130–134 (2013).
132. Montine, T. J. *et al.* Prognostic significance of Ki-67 proliferation index in supratentorial fibrillary astrocytic neoplasms. *Neurosurgery* **34**, 674–678; discussion 678-679 (1994).

133. Alessandrini, F., Ceresa, D., Appolloni, I., Marubbi, D. & Malatesta, P. Noninvasive Monitoring of Glioma Growth in the Mouse. *J. Cancer* **7**, 1791–1797 (2016).
134. Camp, J. G. *et al.* Human cerebral organoids recapitulate gene expression programs of fetal neocortex development. *Proc. Natl. Acad. Sci. U. S. A.* **112**, 15672–15677 (2015).